

NEW INSIGHT INTO STRUCTURAL AND COMPOSITIONAL VARIABILITY IN SOME ANCIENT EXCESS-Ca DOLOMITE

VICTOR A. DRITS

*Geological Institute, Russian Academy of Science, Pyzevskij per. D.7, RU-119017 Moscow, Russia,
and Department of Geological Sciences, The University of Texas at Austin, 1 University Station,
C-1100, Austin, Texas 78712-0254, USA*

DOUGLAS K. MCCARTY[§]

ChevronTexaco, 3901 Briarpark, Houston, Texas 77063, USA

BORIS SAKHAROV

*Geological Institute, Russian Academy of Science, Pyzevskij per. D.7, RU-119017 Moscow, Russia,
and Department of Geological Sciences, The University of Texas at Austin, 1 University Station,
C-1100, Austin, Texas 78712-0254, USA*

KITTY L. MILLIKEN

*Department of Geological Sciences, The University of Texas at Austin, 1 University Station,
C-1100, Austin, Texas 78712-0254, USA*

ABSTRACT

Samples of non-stoichiometric dolomite of different age and origin have been studied by powder X-ray diffraction, scanning electron microscopy and electron-microprobe analysis. Most samples containing a high excess of Ca consist of two or even three phases, differing in the degree of excess Ca uptake and degree of structural order. On the basis of Rietveld refinements of samples with two 3D periodic phases, only the *B* sites have a mixed occupancy of Ca and Mg, and the phases differ from each other only in the content of Ca at the *B* site. A simulation of the experimental XRD patterns of samples showing a high and a low excess of Ca with a defective layer-structure was carried out in terms of mixed-layer structures in which different proportions of nonstoichiometric dolomite layers are interstratified with a small amount of calcite-like as well as stoichiometric dolomite layers. Electron-microprobe analysis and BSE images show that large crystals in the two-phase excess-Ca dolomite samples have sharply bounded zones with different levels of Ca concentrations. Each BSE contrast zone has the same composition (within error), and in each sample there are three or four non-overlapping groups of such zones differing in composition. Remarkably, fine-grained micritic portions of these samples contain the same discrete sets of Ca concentration zones as the large zoned euhedral crystals. This result supports the hypothesis that crystals of excess-Ca dolomite adopt only certain non-continuous compositions, and that growth and composition are structurally controlled.

Keywords: dolomite, excess-Ca dolomite, Rietveld refinement, crystal chemistry, computer simulation, X-ray diffraction, electron-microprobe data.

SOMMAIRE

Nous avons caractérisé des échantillons de dolomite non stoechiométrique d'âges et de provenance différents au moyen de diffraction X sur poudre, microscopie électronique à balayage, et d'analyses effectuées avec une microsonde électronique. La plupart des échantillons contenant un excès appréciable de calcium contiennent deux ou même trois phases, qui diffèrent dans la proportion de l'excédent de Ca et du degré d'ordre structural. D'après nos affinements de Rietveld des spectres de diffraction X des échantillons contenant deux phases à périodicité tri-dimensionnelle, seuls les sites *B* possèdent une occupation mixte de Ca et Mg, et les phases diffèrent entre elles seulement selon le contenu de Ca au site *B*. Une simulation des spectres de diffraction des échantillons de dolomite à faible ou à fort excédent de Ca ayant une structure en feuillets défectueuse comporte une évaluation

[§] *E-mail address:* dmccarty@chevrontexaco.com

des structures à couches mixtes dans laquelle les couches de dolomite non stoechiométrique sont interstratifiées avec une faible quantité de couches ressemblant à la calcite ou à la dolomite stoechiométrique, présentes en proportions différentes. D'après les résultats d'analyses à la microsonde électronique et les images des électrons rétrodiffusés, des domaines volumineux des échantillons de dolomite enrichis en Ca contiennent deux phases bien délimitées, ayant des teneurs en Ca distinctes. Chaque zone ayant un contraste distinct possède la même composition (compte tenu des erreurs expérimentales). Dans chaque échantillon, il y a trois ou quatre groupes distincts de tels domaines à composition distincte. Il est remarquable que les portions micritiques, à granulométrie fine, contiennent les mêmes zones à teneur en Ca distinctes que les cristaux idiomorphes zonés de plus grande taille. Cette observation étaye l'hypothèse voulant que les cristaux contenant un excédent de Ca adoptent seulement certaines compositions non continues, et que la croissance et la composition sont régies par la structure.

Mots-clés: dolomite, dolomite à excédent de Ca, affinement de Rietveld, composition, simulation des spectres, diffraction X, données de microsonde électronique.

INTRODUCTION

In sedimentary rocks, dolomite is commonly nonstoichiometric, containing Ca in excess of its ideal 1 : 1 Ca:Mg ratio. The Ca:Mg ratio may vary over a rather wide range, up to 1.2 : 0.8, *i.e.*, 9–10 mol.% excess CaCO₃ (Goldsmith & Graf 1958, Füchtbauer & Goldsmith 1965, Lumsden 1979, Searl 1994, Budd 1997, Jones *et al.* 2001). Although wide variations in the extent of excess Ca in dolomite are well known, the relationship between diagenetic environment and Ca:Mg ratio remains poorly understood. Variations in Ca:Mg ratio may reflect unique information about mechanisms of crystal growth and conditions of precipitation responsible for dolomite formation and transformation in sedimentary basins.

Application of electron-microprobe analysis shows that some samples of excess-Ca dolomite contain more than one compositional population of dolomite crystals with the same uptake of excess Ca (Searl 1994, Fouke *et al.* 2001). Moreover, individual crystals of dolomite enriched in Ca may consist of several discrete zones differing in Ca:Mg ratio (Fouke & Reeder 1992, Searl 1994, Jones *et al.* 2001).

Recent developments in high-resolution X-ray diffractometry, in Rietveld techniques (Bergman & Kleeberg 1998, Bergman *et al.* 2000), and in algorithms to simulate XRD patterns of defective layer structures (Drits & Sakharov 1976, Plançon 1981, 2002, Drits & Tchoubar 1990, Leoni *et al.* 2004) offer new tools for the examination of structures of Ca-excess dolomite. In addition, cathodoluminescence imaging and back-scattered electron microscopy show that crystals of excess-Ca dolomite may consist of zones with different degrees of Ca-excess, demonstrating compositional heterogeneity of single crystals (Searl & Fallick 1990, Fouke & Reeder 1992, Searl 1994, Jones *et al.* 2001). However, the structural features of such coexistent zones in dolomite differing in level of Ca have not yet been studied.

In the present work, the advantages of these methodologies were used to study the actual structure of samples of ancient excess-Ca dolomite; we document the structural and compositional heterogeneity. Successful solution of the problem was promoted by

integration of powder X-ray diffraction with scanning electron microscopy (SEM) and electron-microprobe analysis.

BACKGROUND INFORMATION

In the structure of dolomite, ideally CaMg(CO₃)₂, there are nonequivalent cation sites, *A* and *B*, each of which is octahedrally coordinated to oxygen atoms of CO₃ groups (Reeder 1983). In dolomite of the above composition, the *A* and *B* sites are occupied by Ca and Mg, respectively, and layers of Ca-bearing octahedra are regularly interstratified with layers of Mg-bearing octahedra, forming the sequence *ABAB*... along the *c* axis of the hexagonal unit-cell. The octahedra are linked by their shared corners. The space group of ideal stoichiometric dolomite structure is *R*3̄.

Most authors assume that excess-Ca dolomite initially formed for kinetic reasons, is less stable, and more soluble than stoichiometric dolomite. A continuous metastable solid-solution series from excess-Ca dolomite to stoichiometric dolomite is postulated to form in response to dissolution–reprecipitation reactions during diagenesis (Lippman 1973, Land 1980, Sperber *et al.* 1984, Mazzullo 1992). In particular, Sperber *et al.* (1984) used this model to explain the global bimodal distribution of the magnitude of excess Ca in a large collection of dolomite compositions.

The energetic consequence of Ca-enrichment was studied by Navrotsky & Capobianco (1987) and Chai *et al.* (1995). These authors used solution calorimetry to show that the enthalpy of formation increases almost linearly with Ca in sedimentary dolomite with Ca-excess ranging from 0 to 6% mole CaCO₃. Their results are in agreement with the conclusion cited above concerning the relative metastability and solubilities of excess-Ca dolomite. The widespread occurrence of excess-Ca dolomite in sedimentary rocks of diverse environments and ages shows, however, that formation and long-term persistence of excess-Ca dolomite reflect kinetic factors rather than energetic ones. It is likely that kinetic controls include such factors as the local compositional heterogeneity of the Ca–Mg solid solution, the extent of Ca–Mg disorder, and various structural and chemical imperfections, among others.

Deciphering the particular kinetic controls on dolomite formation, including a reliable interpretation of a structural mechanism of dolomitization reactions, requires a comprehensive study of the actual crystal structure and composition of dolomite samples having distinct origins.

Two main stages in the intensive characterization of structural and crystal-chemical aspects of dolomite can be distinguished in the literature, although interest in the origin, geochemical and mineralogical features has existed since discovery of this mineral. The first most significant progress in determination of the actual structure of excess-Ca dolomite was achieved in 1950–1970 when the main tool of investigation was powder X-ray diffraction (Bradley *et al.* 1953, Howie & Broadhurst 1958, Steinfink & Sans 1959, Graf 1961, 1969, Goldsmith & Graf 1958, Füchtbauer & Goldsmith 1965, Graf *et al.* 1967, Lippmann 1973).

Goldsmith & Graf (1958) were the first to study structural and compositional variations in ancient sedimentary dolomite using powder and single-crystal X-ray diffraction (XRD). They found that Ca-enrichment of dolomite is accompanied by a significant expansion of the unit-cell parameters. In addition, these authors observed that $h0l$, $0kl$ (l odd) reflections in XRD patterns of Mg-deficient dolomite were usually attenuated with respect to those of stoichiometric dolomite, indicative of disorder in the distribution of Ca and Mg over the structural nonequivalent *A* and *B* sites. The calculated decrease in intensity, however, is smaller than the observed attenuation of the $h0l$, $0kl$ (l odd) reflections, showing that additional imperfections in excess-Ca dolomite contribute to the diffraction pattern observed.

In addition to the attenuation of the $h0l$, $0kl$ (l odd) reflections, Goldsmith & Graf (1958) found variations among excess-Ca dolomite in the intensities of hkl reflections having high and small l . In particular, basal reflections in excess-Ca dolomite were found to be weaker and broader than those in ideal dolomite. The same features were observed for hkl reflections with high l , found to be more diffuse than those with low values of l . For some samples of excess-Ca dolomite, a bimodal distribution of $00l2$ basal reflections was observed. To account for these observations, Graf *et al.* (1967) calculated the positions and intensity of basal reflections for different mixed-layer structural models, with different proportions and different degrees of disorder of magnesite-like and calcite-like layers, where excess of the latter was interstratified. However, these calculations cannot be used for reliable determination of the actual structure of low-temperature sedimentary excess-Ca dolomite. First, careful comparison of positions, shapes, and intensities between calculated and experimental basal reflections was not carried out. Second, even if a satisfactory agreement between the compared data might be achieved, the model cannot be accepted without calculation of hkl reflections.

Despite the fact that samples of dolomite from Recent sediments are characterized by Ca-enrichment and unit-cell expansion, the structural features of these variants differ dramatically from those characteristic of ancient dolomite (Lippmann 1973, Gregg *et al.* 1992, Mazzullo 1992). In XRD patterns of very young samples, the $h0l$, $0kl$ (l odd) reflections are weak in intensity or absent, probably because of a tendency of Ca and Mg to be randomly distributed over the *A* and *B* sites. The other reflections in Recent samples are broad and diffuse, reflecting a low degree of structural order.

The second stage in the structural study of excess-Ca dolomite, and especially of the structural and compositional heterogeneity and microtextures, is related to application of selected-area electron diffraction (SAED), transmission electron microscopy (TEM), and high-resolution transmission electron microscopy (HRTEM) (Reeder 1981, 1983, 1992, Reeder & Wenk 1979, Blake *et al.* 1982, Wenk *et al.* 1983, Barber *et al.* 1985, Wenk & Zhang 1985). These authors showed that all samples of excess-Ca dolomite are characterized by a great diversity of microstructures, including modulations, coherent ribbon-like intergrowths, and superstructures. Excess-Ca dolomite in particular contains lamellar-like structural modulations with wavelengths most commonly ranging from 75 to 200 Å (Reeder & Wenk 1979, Reeder 1983, 1992, Wenk *et al.* 1983, Van Tendeloo *et al.* 1985). These modulations were interpreted as a result of strain originating from local fluctuations in composition or cation order (Reeder 1981, 1992, 2000).

SAED patterns of excess-Ca dolomite commonly contain weak extra spots, which arise from small elongate domains coinciding with modulations (Reksten 1990, Wenk *et al.* 1991, Van Tendeloo *et al.* 1985). Two types of these spots, of so-called *c* and *d* type, were observed. According to Van Tendeloo *et al.* (1985) and Wenk & Zhang (1985), the *c*-type reflections originate from domains in which pure Ca-layers alternate regularly with layers having a mixed $Mg_{0.5}Ca_{0.5}$ composition and an ordered distribution of Ca and Mg along the *a* and *b* axis. The average content of Ca and Mg in the domains responsible for the *c*-type reflections should be equal to $Ca_{1.5}Mg_{0.5}$. Wenk *et al.* (1991) referred to this model as the γ structure. Reksten (1990) assumed that *c*-type reflections arise from the cation order within layers, but supposed that such order takes place in each layer. In this case, the average composition of the domains should be $Ca_{1.0}Mg_{1.0}$. Wenk *et al.* (1991) referred to this model as the ν structure.

The *d*-type extra reflections arise most probably owing to the substitution of a Mg layer by Ca- or Ca-dominated layer forming the defective subsequence of layers $ABAAABA \dots$ (Van Tendeloo *et al.* 1985). Wenk *et al.* (1991) referred this model as the δ structure.

Documentation of the γ , ν , and δ domains leads to a commonly accepted model of excess-Ca dolomite;

these domains are said to occur within a host matrix of stoichiometric dolomite, providing on the one hand Ca-enrichment, and on the other, strains associated with the coherent interface between the matrix and domains that are responsible for the modulations. However, direct information on compositions of ideal dolomite of the host of the Ca-rich ribbon-like domains was obtained by Barber *et al.* (1985) only in saddle dolomite. Therefore, the nature of Ca–Mg order in excess-Ca dolomite remains poorly understood.

Single-crystal refinements of the structure can be an effective tool for the quantitative determination of site occupancies in excess-Ca dolomite. Such refinements have been carried out only for two samples of sedimentary stoichiometric dolomite (Reeder 1983, Miser *et al.* 1987). Calcium and Mg occupy the *A* and *B* sites, respectively. It is worth noting that stoichiometric sedimentary dolomite possessing nearly ideal 3D periodicity with perfect cation order does not contain a modulated structure and superstructures (Wenk *et al.* 1983, Reeder 1983, 1992). Only a single author has undertaken to obtain quantitative determination of site occupancies in excess-Ca dolomite by single-crystal X-ray structural refinement (Reeder 2000). He refined the crystal structure of two samples of excess-Ca dolomite with a pervasive modulation and *c*-type extra reflections. He found that the *A* and *B* sites in their average structures have a mixed Ca–Mg occupancy. Surprisingly, no other such studies have been attempted on pre-Holocene excess-Ca dolomite. No one has examined the nature of the imperfections disturbing the periodic and homogeneous structure of this mineral.

MATERIALS AND METHODS

Samples

Samples were obtained from cores and outcrops at various locations and of different ages. The M236 group of samples was obtained from a core taken in Lea County, New Mexico. This core is in the lower part of the Permian (Leonardian, ~263–268 Ma) Drinkard Formation, deposited near the western shelf margin of the Central Basin platform. Depositional facies of the original limestones include inner-ramp mudstones or wackestones and tidal-flat deposits.

Samples 821–545 and 821–546 are from an outcrop in Coke County, Texas. These samples are from the Cretaceous (Aptian) Edwards Formation. The facies represented by the original limestones are intertidal mudstone or grainstone couplets. Samples designated M214 and 821–511 through 821–516 are from core and are of Lower Mississippian age, from the Lodgepole Formation in Uinta County, Wyoming.

The sample of ankerite (821–548) is from the mineralogical museum in the Russian Academy of Sciences. Sample 821–019 is a laboratory standard of unknown origin. Samples 821–235, 821–391, and 821–534 are

dolomite standards that were obtained from the Wards Scientific Company. The bulk chemical compositions of the samples studied are given in Table 1.

X-ray diffraction

Diffraction scans of each sample were collected with a Thermo Xtra diffractometer and, in some cases, a Scintag X1 diffractometer, both equipped with a solid-state Si detector. Scans were made from various angular ranges, mainly from 20 to 76°2θ (Cu). For Rietveld refinement, samples were scanned from 20 to 140°2θ (Cu). The step increment was 0.01 or 0.02°2θ, and the count rate was 30–40 s per step or longer using CuKα radiation transmitted through a 2.0 mm divergence and 4 mm scatter slit. Detector slits were 0.5 mm and 0.2 mm. To maximize random orientation, diffraction data were obtained after freeze-drying the sample and using a side-loading sample holder (McCarty & Reynolds 1995).

Interpretation of XRD patterns

XRD pattern data were treated by three techniques: 1) careful determination of *hkl* reflection positions to determine the unit-cell parameters, 2) structural refinement by the Rietveld method, and, 3) comparison of the XRD patterns with those calculated for defective-layer structural models of excess-Ca dolomite.

TABLE 1. PROPORTION OF Ca, Mg, Fe AND Mn IN SAMPLES OF EXCESS-Ca DOLOMITE

Sample	Ca	Mg	Fe	Mn
M236-004	1.018	0.980	0.002	0
M236-030	1.029	0.969	0.002	0
M236-038	1.002	0.996	0.002	0
M236-081	1.112	0.884	0.004	0
M236-083	1.064	0.932	0.004	0
M236-104	1.062	0.935	0.002	0
M236-096	1.115	0.883	0.002	0
M236-098	1.090	0.907	0.003	0
M236-116	1.112	0.882	0.006	0
M214-034	1.062	0.936	0.002	0
821-019	1.055	0.911	0.030	0.004
821-235	1.016	0.950	0.025	0.009
821-391	1.024	0.965	0.009	0.002
821-511	1.067	0.932	0.001	0
821-512	1.043	0.957	0	0
821-513	1.039	0.960	0.001	0
821-514	1.045	0.954	0.001	0
821-515	1.043	0.957	0	0
821-516	1.031	0.969	0	0
821-549	1.084	0.893	0.022	0
821-551	1.070	0.915	0.015	0
821-534	1.020	0.958	0.022	0
821-545	1.098	0.902	0	0

Units: atoms per formula unit (*apfu*).

Determination of hkl peak positions

This procedure includes the following steps: 1) calibration of *hkl* peak positions using those of Si as an internal standard, 2) removing the contribution of $K\alpha_2$ from each *hkl* peak mathematically, and 3) simulation of the profile of each individual *hkl* peak corresponding to $K\alpha_1$ to determine its position (2θ) and d value. Our experience shows that this procedure is especially effective for the decomposition of a profile consisting of two closely located diffraction-maxima. A pseudo-Voigt function provides a good approximation of the shape of the reflections. The Jade[®] computer program (MDI, Inc.) was used for this treatment of the data.

The Rietveld technique

This method, initially proposed by Rietveld (1969), has been significantly improved during last two decades to become an effective tool for reliable structural analysis of various compounds having 3D order.

In the present work, the computer program BGMN for structural refinements by the Rietveld method developed by Bergman & Kleeberg (1998) and Bergman *et al.* (2000) was used. One advantage of this program is that influences on peak shape arising from instrumental factors *versus* those from the sample itself are discriminated by taking into account the tube-tail effect. A small portion of the X-rays emitted by the tube originate not inside the focus but up to 1 mm beyond the focus. This means 1 mm equatorial broadening toward both sides of the optical focus. If not corrected, these tube-tails may totally disturb the profile shapes. Therefore, before using the program, the tube-tail effect was measured for the particular tube used in the diffractometer and then was taken into account for simulation of the experimental XRD patterns.

In a totally new algorithm for mathematical refinement, optional boundaries can be introduced for each parameter. Therefore, the program converges in each case. Finally, structural refinement can be carried out for several coexisting phases with parallel quantitative phase-analysis. The quality of fit for experimental and calculated profiles obtained by the program was checked using the observed XRD patterns from LaB₆ and Si standards.

Simulation of XRD patterns from defective-layer structural models

The presence of stacking faults and interstratification effects commonly prevents the crystal-chemical study of layered minerals by conventional methods of structural analysis, including the Rietveld technique. Indeed, among the available Rietveld refinement algorithms, only BGMN employs a non-trivial algorithm to account for the stacking features typical for layer silicates (Bergman & Kleeberg 1998, Bergman *et al.*

2000). However, even in this case, only a few details related to stacking disorder can be refined. An effective way to obtain structural and crystal-chemical information from defective minerals is to simulate diffraction effects from realistic structural models and to then compare the calculated and observed XRD patterns (Drits & Sakharov 1976, Drits & Tchoubar 1990). This approach has been successfully applied to natural and synthetic phyllosilicates (Plançon *et al.* 1989, Sakharov *et al.* 1990, Reynolds 1993, McCarty & Reynolds 1995, 2001, Manceau *et al.* 2000, Drits *et al.* 1993, Gualtieri 1999, Cuadros & Altaner 1998, Ylagan *et al.* 2000), phylломanganates (Drits *et al.* 1998, Lanson *et al.* 2000, 2002, Manceau *et al.* 1997, Gaillot *et al.* 2004), and zeolites (Newsam & Treacy 1993, Braunbarth *et al.* 2000). The mathematical formalism used to calculate powder-diffraction patterns was described by Plançon & Tchoubar (1977), Plançon (1981, 2002), Sakharov *et al.* (1982) and, in greater detail, by Drits & Tchoubar (1990).

A principal advantage of this approach is that it can predict diffraction effects from diverse theoretically possible and crystal-chemically justified structural models. Its application allows us to analyze diffraction effects of various parameters peculiar to periodic and defective structural models. Comparison of the experimental XRD patterns with those calculated for different structural models makes it possible to determine the nature of interstratified types of layers or stacking faults, their contents, and distribution pattern. For each particular model, the following structural and probability parameters should be defined: 1) the structural and chemical composition of coexisting layers, 2) the azimuthal orientations, translations, reflection operations, and patterns of alternation of the layers, 3) probability parameters that describe quantitatively the model (*e.g.*, proportion of each type of layer, w_i , and conditional probability, p_{ij} , denoting the probability of the layer type j to follow layer type i , where the short-range factor is equal to 1). We assume that the interstratification of the layer types follows Markovian statistics (Drits & Tchoubar 1990).

Whole-rock elemental analysis

Major- and trace-element data on bulk samples were obtained by XRAL Laboratories, Toronto, Canada using by inductively coupled plasma – atomic emission spectroscopy (ICP–AES) and, in some cases, X-ray fluorescence (XRF) spectroscopy.

Bulk composition by electron-microprobe analysis

In the analysis of dolomite by wavelength-dispersion spectrometry (WDS), we employed a 10 μm spot, a 12 nA sample current (as measured on brass), and 20-second count times for all elements. Dolomite (Mg, Ca), siderite (Fe, Mn), and Sr-glass standards in the

collection of the University of Texas at Austin Electron Microprobe Laboratory were used for calibrations. The same dolomite and siderite, and a Sr-rich coral were used as secondary standards. We used back-scattered electron imaging to inspect the compositional heterogeneity of the samples analyzed and as a guide for precise placement of the beam prior to each analysis.

Scanning electron microscopy

A Philips model XL-20 scanning electron microscope (SEM) equipped with an EDAX energy-dispersion spectrometer (EDS) was used to obtain complementary semiquantitative chemical data and magnified images of the samples under study.

Stable isotope analyses

Approximately 250 μg of crushed sample was reacted at 90°C with H_3PO_4 for 20 minutes in a Micro-mass MultiPrep automated preparation system. The assumed phosphoric acid fractionation factor between dolomite and CO_2 is taken to be 1.0090. The evolved CO_2 was analyzed on a VG PRISM II mass spectrometer in the Stable Isotope Lab, Department of Geological Sciences, The University of Texas at Austin. The data were normalized to accepted values for in-house calcite standards included within the batch of samples.

Sr isotopic analyses

To minimize the contribution of Sr from sources other than from within the sample, approximately 50 mg of crushed rock was reacted with 1 M ammonium acetate, rinsed in de-ionized water, then given a final rinse in 1% acetic acid, prior to dissolution in 8% acetic acid for 30 minutes. Any insoluble residue was removed by centrifugation. Strontium was isolated using Sr-specific resin, then loaded onto zone-refined Re filaments along with Ta_2O_5 . Proportions of the isotopes of Sr were established on a Finnigan MAT 261 mass spectrometer at the Department of Geological Sciences, the University of Texas at Austin, operated in dynamic multicollection mode. The exponential law was used to correct for fractionation. The blank for this procedure was 21 pg of Sr.

RESULTS

Qualitative analysis of XRD patterns

On the basis of XRD patterns, the samples of excess-Ca dolomite can be separated into two main groups. Samples of the first group consist of single-phase dolomite in which the excess Ca is relatively small (0.04–0.05 atoms per formula unit, *apfu*). In the second group, Ca-excess is typically greater than 0.05 atoms per formula and includes samples that contain at least

two dolomite phases. For example, Figure 1a shows an XRD pattern from sample M236–116 recorded using $K\alpha_1 + K\alpha_2$ radiations. One can see that *hkl* reflections of one coexistent phase almost coincide with $K\alpha_2$ maxima of the other phase. Nevertheless, the coexistence of two phases in this sample can be recognized unambiguously. This is even more evident if the $K\alpha_2$ contribution is subtracted (Fig. 1b).

If the difference between unit-cell parameters of coexisting dolomite phases is small, subtraction of the $K\alpha_2$ contribution from the XRD pattern is an important approach for their discrimination. For example, XRD patterns from sample 821–081 (Figs. 1c, d) illustrate the efficiency of this approach. With the $K\alpha_2$ contribution subtracted, the remaining closely located and rather well-resolved *hkl* reflections clearly demonstrate the existence of the two dolomite phases. Coexistent phases having smaller and larger unit-cell parameters will be referred as phase I and phase II, respectively. Accordingly, reflections of these phases having the same *hkl* are located at higher and lower 2θ angles, respectively.

Samples within this second group of multiphase samples of dolomite are characterized by a huge diversity of diffraction features. Goldsmith & Graf (1958) showed that the XRD regions that most effectively demonstrate a diffraction variety of excess-Ca dolomite contain *006* and *110* reflections on one hand, and the *0012* and *030* reflections on the other. Figure 2 shows these fragments, which reflect the most characteristic diffraction features of the samples studied. The first low- 2θ -angle region along with *006* and *110* contains also *015* and *113* reflections, whereas the other part also contains *217* and *0210* reflections. As can be seen in Figure 2a, samples M236–116, M236–098, 821–545, and M236–073 are characterized by XRD fragments in which each of the pairs of reflections having the same *hkl* is well distinguished, and their positions can be determined with a high precision by peak decomposition. For some samples, the presence of two dolomite phases in the low- 2θ region is observed only because of the splitting of the *006* and *015* reflections, whereas the *110* and *113* reflections seem rather narrow and symmetrical (sample M236–073). However, in the high- 2θ region, not only the *0012*, *217* and *0210* reflections, but also the *030* reflection show a bimodal distribution of intensity (Fig. 2b). The two phases thus differ from each other in both *a* and *c* unit-cell parameters. In addition, comparison of the intensity of reflections having the same *hkl* reflections and located in the higher- and lower- 2θ regions shows that the proportions of the phases in the samples studied are different. For example, one can see that the contents of phases I and II in sample M236–116 are similar, whereas in sample 821–545, phase II prevails.

Even visual observation shows that the profiles of *006* and *015* reflections corresponding to different phases may be vastly different. For example, in the XRD fragments shown for samples M236–081 and

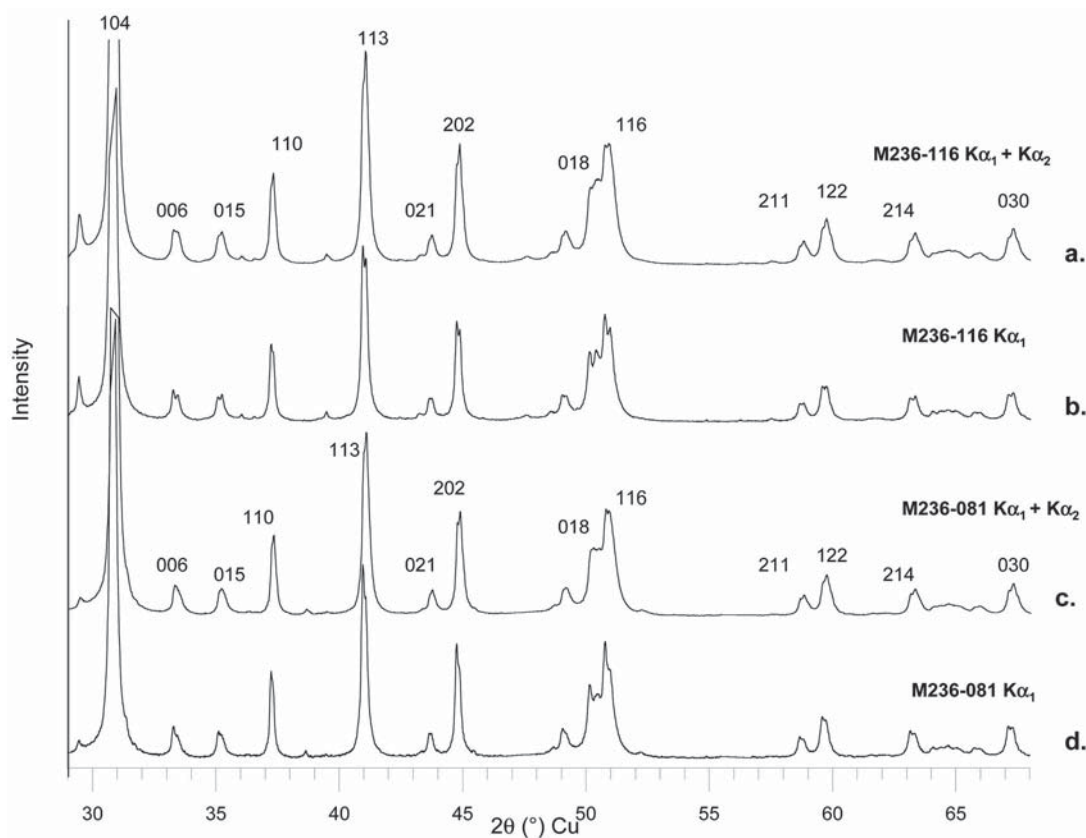


FIG. 1. Powder XRD patterns from the two-phase samples M236-116 and M236-081 recorded using $K\alpha_1 + K\alpha_2$ radiations (a and c) and those in which the contribution of $K\alpha_2$ radiation is subtracted (b and d).

M236-096, the reflections corresponding to phase II are significantly narrower and more intense than the reflections of phase I, which appear wider and weaker. One of the possible explanations is that sizes of coherent scattering domains (CSD) of phase II are significantly larger than those of phase I. An alternative interpretation is that the wide and weak reflections consist of two closely located maxima.

Peculiar diffraction-effects are observed for sample 821-019 (Fig. 2). In the low- 2θ region, the 006 and 015 reflections are split into pairs. This sample thus consists of two phases different from each other at least in the c parameter, because the 110 and 113 reflections are rather narrow and symmetrical (Fig. 2a). By analogy with the other samples described above, one might expect that in the high- 2θ region, the 0012 reflections should be separated by an even wider 2θ interval. In contrast, as can be seen in Figure 2b, the 0012 reflection profile is much narrower than those observed for 0012 reflections of the other samples. It seems that one of the expected basal reflections has zero intensity. A

similar feature is observed for the 217 and 0210 reflection profiles. They are much narrower than profiles of the 217 and 0210 reflections observed from the samples described above.

Similar speculations may be applied to interpret diffraction effects from samples 821-549 and 821-551. In the low- 2θ region, the 006 , 015 , 110 and 113 reflections are intense, and have only slightly asymmetrical profiles, which may reveal the presence of two phases (Fig. 2a). In contrast, asymmetrical shapes of 0012 , 217 and 0210 maxima strongly increase in the high- 2θ region, whereas the 030 peak remains almost symmetrical. Such diffraction features may reflect either coexistence of several dolomite phases having different c but identical or very similar a parameters, or the existence of some specific defects providing an asymmetrical profile of hkl reflections with high l . An alternative explanation is a combination of both phase heterogeneity and structural defects. The fact that the phases I and II may differ from each other in their relative proportions, extent of Ca-excess, and the unit-

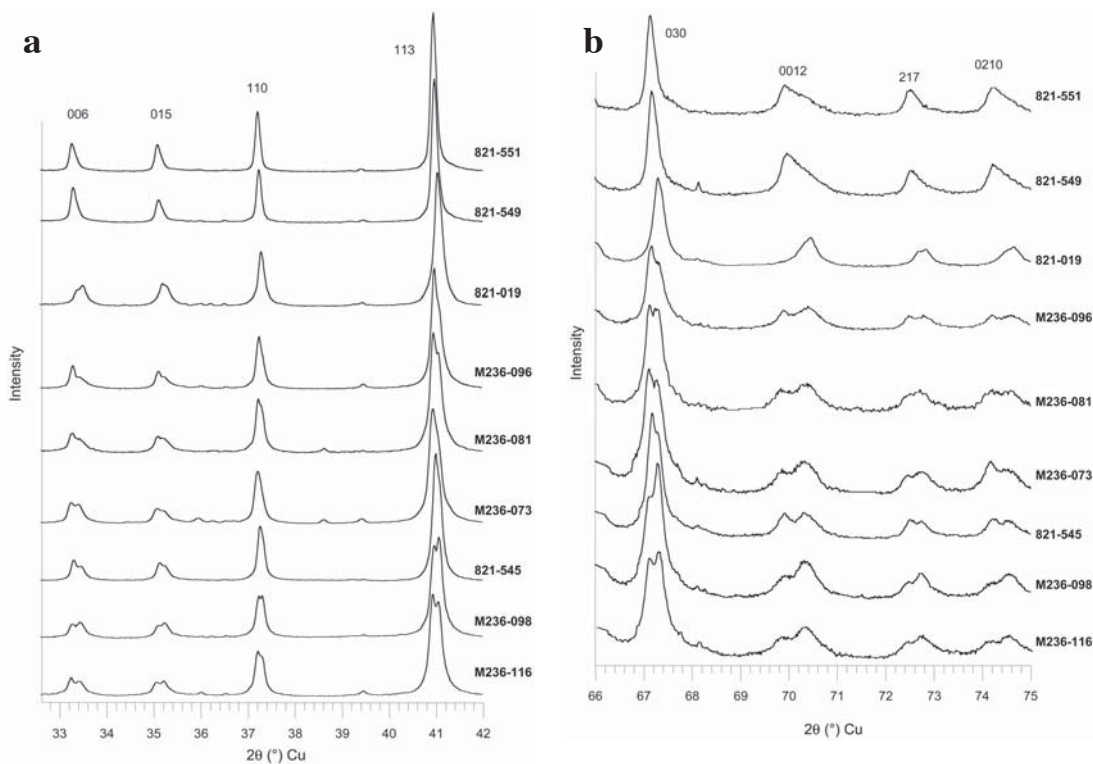


FIG. 2. Low- 2θ (a) and high- 2θ (b) angle fragments of powder XRD patterns from the samples studied (see details in the text).

cell parameters is well illustrated by a set of the XRD pattern fragments containing 018 and 116 reflections overlapping in different fashions (Fig. 3).

Determination of unit-cell parameters

Careful determination of hkl reflection positions using internal standards, in combination with simulation of individual reflection profiles, provide a high precision of the measured $d(hkl)$ values with an average accuracy $\pm(2 \text{ to } 3) \times 10^{-4}$ Å. The least-squares technique was used to determine the unit-cell parameters for both monophase and two-phase samples of excess-Ca dolomite. The refinements of unit-cell parameters have shown that samples of the single-phase excess-Ca dolomite form two main groups. One of them includes phases for which the measured and calculated $d(hkl)$ values coincide within the experimental errors. For these samples, standard deviations for the refined unit-cell parameters are equal to $0.0002\text{--}0.0006$ Å for a , and $0.005\text{--}0.001$ Å for c cell parameters. This group consists mostly of monophase excess-Ca dolomite containing a relatively low excess of Ca ($0.01\text{--}0.05$ apfu), for example, samples M286-001, M236-030, 821-016, 821-235, 821-391, and 821-512 to 821-514. We found

only a few samples (*e.g.*, sample 236-128) that contain a high excess of Ca (0.09 apfu) for which $d_{\text{exp}}(hkl)$ and $d_{\text{calc}}(hkl)$ almost coincide within experimental errors.

For the second group of single-phase excess-Ca dolomite, the refined unit-cell parameters provide good agreement between the compared $d(hkl)$ values only for some of the hkl reflections. Comparison of the experimental $d(hkl)$ with those calculated from the refined unit-cell parameters of samples M214-034 and M236-104 is remarkable in this respect (Table 2). In contrast to the samples of the first group, the experimental and calculated positions of the reflections in these samples almost coincide only for hkl reflections with low l . However, a significant disagreement between the compared values of 2θ is observed for hkl reflections with high l . For example, for the 0012 reflection of sample M214-034, this difference is equal to $0.081^\circ 2\theta$. Similar disagreement between $2\theta_{\text{exp}}$ and $2\theta_{\text{calc}}$ is observed for 018 , 208 , 119 , 217 , 0210 , among others (Table 2). These observed regularities are widespread among samples of excess-Ca dolomite, even where they contain relatively low levels of excess Ca.

A common feature of the experimental XRD patterns of both groups of excess-Ca dolomite, noted earlier by Goldsmith & Graf (1958), is reflection broadening

depending significantly on hkl . In particular, for a given hk , this effect increases with l , whereas for each given l , the reflection width increases with $(h^2 + k^2)$. For example, even in the samples of ordered dolomite, the values of full width at half maximum (FWHM) of 0012 reflections are twice of those of 006 ones.

Samples containing two excess-Ca dolomite phases deserve special consideration. It is clear that these phases differ from each other in the content of Ca. Therefore, for each given pair of reflections having the same hkl , the higher value of the spacing corresponds to the phase with higher content of Ca. Therefore, higher excess-Ca and lower excess-Ca phases correspond to phase II and phase I, respectively.

As mentioned above, decomposition of the profiles of each pair of hkl reflections allows us to determine their positions with high precision and then, with the least-squares method, to refine the unit-cell parameters of both phases (Table 3). We should stress that the

unit-cell parameters of phase II of the samples studied provide perfect agreement between the observed and calculated positions of peaks (2θ) and $d(hkl)$, independent of the hkl reflection. To illustrate, Table 4 shows deviations between experimental and calculated positions ($\Delta^\circ 2\theta$) and spacings [$\Delta d(hkl)$] obtained for the phase II of sample M236–116. The mean value of $\Delta^\circ 2\theta$ is less than $0.01^\circ 2\theta$, with the mean $\Delta d \leq 0.0002$ Å. For the phase studied, its average structure has 3D periodicity, *i.e.*, it does not contain significant imperfections disturbing this periodicity.

However, the periodicity of the phase-I structure is not invariably perfect, and the degree of its imperfections varies from sample to sample. We found, in particular, that for phase I of some samples, the positions of the 006 and 0012 reflections do not obey Bragg's law. If, for example, one assumes that the position of the 006 reflection corresponds to the actual one, then the observed 0012 peak is significantly shifted to

TABLE 2. THE REFINED UNIT-CELL PARAMETERS, EXPERIMENTAL POSITIONS ($2\theta_{\text{exp}}$), EXPERIMENTAL (d_{exp}) AND CALCULATED (d_{calc}) VALUES, THE DIFFERENCES BETWEEN THE EXPERIMENTAL AND CALCULATED POSITIONS ($\Delta 2\theta$) AND d -VALUES (Δd) OF hkl REFLECTIONS FOR SAMPLES M214–034 AND M236–104

sample unit-cell parameters	M214-034 a 4.8133(4), c 16.034(3) Å					M236-104 a 4.8138(4), c 16.0478(32) Å				
	hkl	$2\theta_{\text{exp}}^\circ$	$\Delta(2\theta)^\circ$	d_{exp} Å	d_{calc} Å	Δd Å	$2\theta_{\text{exp}}^\circ$	$\Delta(2\theta)^\circ$	d_{exp} Å	d_{calc} Å
104	30.913	0.011	2.8903	2.8893	-0.0010	30.900	0.008	2.8915	2.8908	-0.0007
006	33.489	0.011	2.6728	2.6723	-0.0005	33.454	0.022	2.6764	2.6746	-0.0018
015	35.273	0.010	2.5424	2.5417	-0.0007	35.259	0.012	2.5433	2.5425	-0.0008
110	37.332	0.001	2.4067	2.4067	0.0000	37.327	0.009	2.4075	2.4069	-0.0006
113	41.098	0.001	2.1945	2.1944	0.0001	41.087	0.002	2.1951	2.1949	-0.0002
021	43.764	-0.001	2.0668	2.0668	0.0000	43.761	-0.003	2.0669	2.0671	0.0002
202	44.903	-0.005	2.0170	2.0172	0.0002	44.886	0.006	2.0177	2.0175	-0.0002
024	49.228	0.005	1.8494	1.8492	0.0002	49.223	-0.003	1.8496	1.8497	0.0001
018	50.514	-0.030	1.8053	1.8063	0.0010	50.499	-0.051	1.8058	1.8075	0.0017
116	51.020	0.007	1.7886	1.7883	-0.0002	51.001	0.003	1.7892	1.7891	-0.0001
211	58.853	-0.007	1.5678	1.5680	0.0002	58.843	-0.003	1.5681	1.5681	0.0000
122	59.772	-0.003	1.5459	1.5460	0.0001	59.766	-0.005	1.5460	1.5461	0.0001
214	63.386	-0.007	1.4662	1.4663	0.0001	63.375	-0.011	1.4664	1.4666	0.0002
208	64.483	-0.040	1.4439	1.4447	0.0008	64.459	-0.052	1.4443	1.4454	0.0011
119	65.133	-0.046	1.4310	1.4319	0.0009	65.079	-0.035	1.4321	1.4328	0.0007
125	66.010	0.001	1.4141	1.4141	0.0000	66.004	-0.010	1.4142	1.4144	0.0002
030	67.333	0.001	1.3895	1.3895	0.0000	67.338	-0.011	1.3894	1.3896	0.0002
0012	70.489	-0.081	1.3348	1.3362	0.0013	70.490	-0.150	1.3350	1.3373	0.0023
217	72.829	-0.033	1.2976	1.2981	0.0005	72.794	-0.026	1.2981	1.2985	0.0004
0210	74.670	-0.052	1.2701	1.2708	0.0008	74.610	-0.042	1.2710	1.2716	0.0006

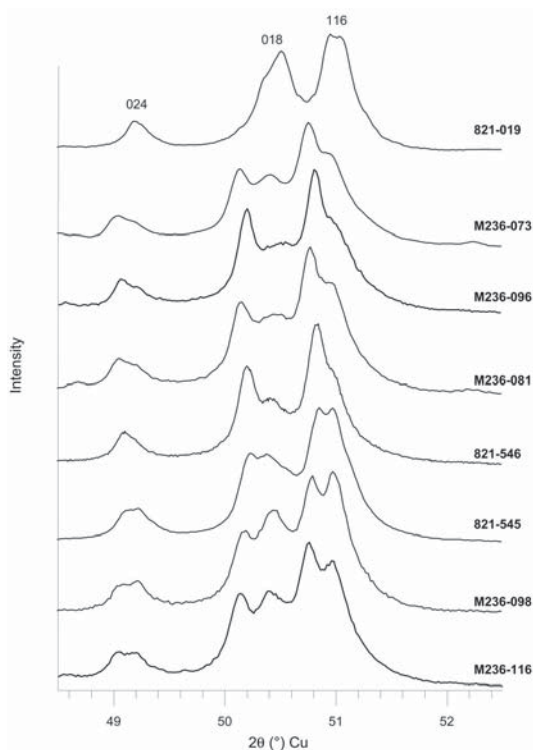


FIG. 3. Diffraction data showing the variation in the position, shape, and intensity of two pairs of hkl reflections having 018 and 116 indices, corresponding to phases I and II.

higher 2θ angles in comparison with that predicted by Bragg's law [$d(0012) = d(006)/2$]. Refinement of the unit-cell parameters of phase I for some of the samples studied shows that calculated positions of 006 and 0012 reflections are shifted with respect to the experimental ones to the lower and higher 2θ angles, respectively. This difference increases with increasing deviation of the 006 and 0012 reflections from Bragg's law, which can be expressed as a difference between $d(006)_{\text{exp}}/2$ and $d(0012)_{\text{exp}}$ or as $\Delta 2\theta(006) - \Delta 2\theta(0012)$, where $\Delta 2\theta$ is the difference between 2θ corresponding to the calculated and experimental positions of $00l$ reflections. These differences have minimal values for the phase I of samples M236-116 and M236-098 ($\Delta d \leq 0.0005$ Å and $\Delta 2\theta \approx 0.034^\circ$) and become significant for this phase in samples 821-546, M236-083, and M236-073 (Δd increases up to 0.003 Å and $\Delta 2\theta$ up to $0.13^\circ 2\theta$) (Tables 4, 5).

In fact, there are two groups of samples of defective excess-Ca dolomite. For one of them, only $00l$ reflections do not obey Bragg's law (sample M236-073, phase 1, Table 5), whereas for the other one (as was found for the defective monophase excess-Ca dolo-

mite), a general agreement between the compared $2\theta(hkl)$ and $d(hkl)$ depends not only on $00l$, but also on hkl . In particular, the disagreement between the measured and calculated 2θ and $d(hkl)$ increases with l (sample M236-083, phase 1, Table 5).

Table 3 shows that the unit-cell parameters values of phases I and II vary over a rather narrow interval despite the fact that they come from different geological environments. For example, the a_2 and c_2 parameters corresponding to phase II vary over the intervals 4.822 – 4.829 Å and 16.124 – 16.159 Å, respectively. Similarly, the a_1 and c_1 parameters of phases I vary over the intervals 4.8134 – 4.8159 Å and 16.051 – 16.072 Å, respectively. Sample 821-019 is exceptional, because its a_2 and c_2 parameters are similar to a_1 and c_1 of phase I of the other two-phase samples (Table 3). Nevertheless, even for this sample, the a and c parameters of phase II are greater than those of phase I. It is remarkable that for this sample, not phase I, but phase II has a significant disagreement between the experimental positions of 006 and 0012 reflections, and those calculated from the refined unit-cell parameters (Table 5).

DETERMINATION OF THE DEGREE OF CA-MG ORDER IN PHASES I AND II BY THE RIETVELD TECHNIQUE

The coexistence of two phases having 3D periodic structure in the same sample seems unusual, especially considering the commonly accepted view that most excess-Ca dolomite should have a defective structure. Therefore, one of the objectives of our study was to investigate by the Rietveld technique the degree of Ca-Mg order in these phases and to determine the nature of cation order in phases I and II. As a first step, a structural refinement was carried out for ankerite, an isostructural variety of dolomite in space group $R\bar{3}$. The composition of this and other refined samples is given in Table 6. Our aim was to test the distribution of Ca, Mg, and Fe cations over the A and B sites and to compare the cation occupancies of these sites with the average composition determined by chemical analysis.

TABLE 3. REFINED UNIT-CELL PARAMETERS FOR Ca-PHASES I AND II OF THE SAMPLES STUDIED

Sample	a_1 (Å)	c_1 (Å)	a_2 (Å)	c_2 (Å)
M236-116	4.8159(3)	16.0633(13)	4.82927(32)	16.1593(11)
M236-073*	4.8152(7)	16.060(2)	4.8280(3)	16.159(1)
M236-098	4.81338(5)	16.05136(24)	4.82572	16.13612(12)
M236-081	4.81338(55)	16.05198(24)	4.82661	16.14924(31)
821-545	4.81437(51)	16.0513(12)	4.82326(14)	16.13177(44)
821-546	4.8136(7)	16.0527(16)	4.82239(21)	16.12836(65)
821-019**	4.8076(35)	16.0225(60)	4.8146(3)	16.0402(34)
821-549*	4.8148(16)	16.0724(20)	4.8238(18)	16.1240(2)

* $00l$ reflection positions of phase I do not strictly obey Bragg's law.

** $00l$ reflection positions of phase II do not obey Bragg's law.

TABLE 4. THE REFINED UNIT-CELL PARAMETERS, EXPERIMENTAL POSITIONS ($2\theta_{exp}$), EXPERIMENTAL (d_{exp}) AND CALCULATED (d_{calc}) VALUES, THE DIFFERENCES BETWEEN THE EXPERIMENTAL AND CALCULATED POSITIONS ($\Delta 2\theta$) AND d -VALUES (Δd) OF hkl REFLECTIONS FOR SAMPLE M236-116

unit-cell parameters	a 4.82927(32), c 16.1593(11) Å phase II					a 4.8159(3), c 16.0633(13) Å phase I				
	hkl	$2\theta_{exp}^\circ$	$\Delta(2\theta)^\circ$	d_{exp} Å	d_{calc} Å	Δd Å	$2\theta_{exp}^\circ$	$\Delta(2\theta)^\circ$	d_{exp} Å	d_{calc} Å
104	30.746	-0.001	2.9056	2.9056	0.0000	30.881	0.004	2.8932	2.8928	-0.0004
006	33.239	-0.001	2.6931	2.6932	0.0001	33.439	0.004	2.6775	2.6772	-0.0003
015	35.064	-0.004	2.5570	2.5573	0.0003	35.228	0.005	2.5455	2.5451	-0.0004
110	37.213	-0.007	2.4142	2.4146	0.0004	37.318	-0.006	2.4076	2.4080	0.0004
113	40.926	-0.001	2.2033	2.2034	0.0001	41.067	-0.001	2.1961	2.1961	0.0000
021	43.613	0.006	2.0736	2.0738	0.0002	43.746	-0.009	2.0676	2.0680	0.0004
202	44.725	0.003	2.0246	2.0244	-0.0002	44.866	0.002	2.0185	2.0184	-0.0001
024	49.010	0.000	1.8571	1.8571	0.0000	49.198	-0.007	1.8505	1.8507	0.0002
018	50.106	0.004	1.8190	1.8189	-0.0001	50.398	0.000	1.8092	1.8092	0.0000
116	50.729	0.009	1.7982	1.7974	-0.0003	50.971	-0.005	1.7902	1.7903	0.0001
211	58.632	-0.001	1.5732	1.5332	0.0000	58.813	-0.003	1.5688	1.5689	0.0001
122	59.540	0.000	1.5513	1.5513	0.0000	59.733	-0.003	1.5468	1.5469	0.0001
214	63.104	-0.001	1.4721	1.4721	0.0000	63.325	0.002	1.4674	1.4674	0.0000
208	64.043	-0.006	1.4527	1.4528	0.0001	64.350	0.005	1.4465	1.4464	-0.0001
119	64.638	-0.002	1.4408	1.4408	0.0000	64.960	0.026	1.4344	1.4339	-0.0005
125	65.693	0.008	1.4200	1.4202	-0.0002	65.965	-0.013	1.4150	1.4152	0.0002
030	67.081	0.000	1.3941	1.3941	0.0000	67.291	0.001	1.3903	1.3903	-0.0000
0012	69.790	-0.009	1.3465	1.3465	0.0000	70.290	-0.030	1.3381	1.3386	0.0005
217	72.381	-0.010	1.3045	1.3047	0.0002	72.735	-0.020	1.2990	1.2993	0.0003
0210	74.100	-0.013	1.2784	1.2786	0.0002	74.540	-0.041	1.2721	1.2726	0.0005

TABLE 5. THE REFINED UNIT-CELL PARAMETERS, EXPERIMENTAL POSITIONS ($2\theta_{exp}$), EXPERIMENTAL (d_{exp}) AND CALCULATED (d_{calc}) VALUES, THE DIFFERENCES BETWEEN THE EXPERIMENTAL AND CALCULATED POSITIONS ($\Delta 2\theta$) AND VALUES (Δd) OF hkl REFLECTIONS FOR SAMPLES M236-073, M236-083 AND 821-019

Sample	M236-073, phase I					M236-083, phase I					821-019, phase II				
	Unit-cell parameters	a 4.8152 (8), c 16.060(2) Å					a 4.8143(44), c 16.0444(27) Å					a 4.8146(3), c 16.0402(34) Å			
hkl	$2\theta_{exp}^\circ$	$\Delta(2\theta)^\circ$	d_{exp} Å	d_{calc} Å	Δd Å	$2\theta_{exp}^\circ$	$\Delta(2\theta)^\circ$	d_{exp} Å	d_{calc} Å	Δd Å	$2\theta_{exp}^\circ$	$\Delta(2\theta)^\circ$	d_{exp} Å	d_{calc} Å	Δd Å
104	30.890	0.000	2.8924	2.8924	0.0000	30.901	0.008	2.8914	2.8906	-0.0008	30.876	0.010	2.8932	2.8937	0.0005
006	33.424	0.025	2.6787	2.6767	-0.0200	33.462	0.021	2.6757	2.6741	-0.0016	33.422	-0.002	2.6788	2.6790	0.0002
015	35.52	-0.013	2.5438	2.5447	0.0009	35.241	0.024	2.5446	2.5429	-0.0017	35.222	-0.002	2.5459	2.5461	0.0002
110	37.321	-0.003	2.4078	2.4076	0.0002	37.321	0.004	2.4074	2.4072	-0.0002	37.321	-0.004	2.4074	2.4077	0.0003
113	41.062	0.010	2.1963	2.1958	-0.0005	41.085	0.001	2.1951	2.1951	0.0000	41.070	-0.005	2.1959	2.1961	0.0002
021	43.751	0.008	2.0674	2.0671	-0.0003	43.763	-0.011	2.0668	2.0673	0.0005	43.768	0.004	2.0680	2.0678	-0.0002
202	44.871	0.004	2.0183	2.0181	-0.0002	44.881	0.005	2.0179	2.0177	-0.0002	44.875	-0.003	2.0182	2.0183	0.0001
024	49.202	-0.003	1.8503	1.8504	-0.0001	49.223	0.005	1.8496	1.8498	0.0002	49.188	0.000	1.8508	1.8508	0.0000
018	50.406	0.001	1.8089	1.8089	0.0000	50.483	-0.031	1.8063	1.8073	0.0010	50.365	0.005	1.8103	1.8101	-0.0002
116	50.983	-0.008	1.7898	1.7901	0.0003	50.998	0.007	1.7893	1.7891	-0.0002	50.961	0.007	1.7905	1.7908	0.0003
211	58.837	-0.017	1.5682	1.5686	0.0004	58.844	-0.012	1.5680	1.5683	0.0003	58.820	-0.002	1.5686	1.5687	0.0001
122	59.743	-0.003	1.5466	1.5467	0.0001	59.761	-0.008	1.5461	1.5463	0.0002	59.734	0.002	1.5468	1.5467	-0.0001
214	63.342	-0.004	1.4671	1.4672	0.0001	63.364	-0.005	1.4666	1.4667	0.0001	63.332	0.004	1.4673	1.4674	0.0001
208	64.344	0.023	1.4466	1.4461	-0.0005	64.400	0.010	1.4455	1.4453	-0.0002	64.340	0.006	1.44467	1.4468	0.0001
119	65.022	-0.024	1.4330	1.4336	0.0006	65.097	-0.046	1.4317	1.4326	0.0009	65.021	-0.016	1.4332	1.4344	0.0012
125	65.948	0.016	1.4153	1.4150	-0.0003	65.979	0.010	1.4147	1.4145	-0.0002	65.940	0.010	1.4154	1.4156	-0.0002
030	67.294	0.009	1.3902	1.3900	-0.0002	67.324	-0.007	1.3897	1.3898	0.0001	67.300	0.001	1.3901	1.3901	0.0000
0012	70.299	-0.025	1.3380	1.3384	0.0004	70.466	-0.111	1.3352	1.3370	0.0018	70.466	-0.090	1.3352	1.3395	0.0043

In Table 6, we list the refined unit-cell parameters as well as the refined positions and occupancies of the *A* and *B* sites for this sample. In Figure 4, we show the experimental and calculated XRD patterns for the ankerite. As expected, the *A* site is occupied by Ca, whereas the cation composition of the *B* site is in agreement with the average composition (Table 6). The interatomic distance Ca–O, equal to 2.378 Å (Table 6), coincides within errors for that determined for ankerite (Reeder & Dollase 1989). The (Fe,Mg)–O bond length is equal to 2.094 Å, in agreement with cation occupancy at the *B* sites. In particular, taking into account that in ankerite the content of Fe at the *B* sites is equal to 0.33 *apfu* and Fe²⁺–O = 2.12 Å and Mg–O = 2.08 Å, then the expected (Fe,Mg)–O distance should be equal to 2.093 Å. This value coincides within error with the refined length of (Fe,Mg)–O, 2.094 Å (Table 6). These results show that the BGMN program correctly takes into account preferred orientation, shape, and distribution of microcrystals, as well as instrumental factors, providing reliable information about the average structural parameters of the ankerite sample studied.

Application of the method to the two-phase excess-Ca dolomite shows that results that are acceptable from the crystal-chemical point of view are obtained, first, if the relative contents of the coexisting phases are compatible and, second, if their unit-cell parameters differ from each other strongly enough to provide such resolution of the reflections having the same *hkl* where at least the tops of these reflections are sufficiently separated to be

seen. We found that the *A* sites in the refined structures of both phases are occupied only by Ca, whereas the excess Ca is located at the *B* sites. For example, Table 6 lists positional coordinates for atoms and selected interatomic distances for the various polyhedra refined for both phases in samples M236–116, M236–098 and 821–545. Refinement of each phase was carried out in space group *R*3̄, with *R*_{wp} residuals varying from 5.86 to 6.87% (Table 6, Fig. 4). These values are comparable with that determined for the refined ankerite (5.24%). Occupancies of the *A* and *B* sites were refined using constraints of the total Ca-excess in each of the refined phases as determined from the results of the electron-microprobe analysis (see below).

Because of the uncertainties in the determination of crystal-size distributions and profile modeling, a common problem in the Rietveld refinement is that the values of the esd of the atom coordinates are significantly underestimated. However, the bond lengths and occupancies of the *B* sites are not far from the expected ones. In particular, the average total content of Ca in both phases of each sample [*W*₁(P^B_{Ca})₁ + *W*₂(P^B_{Ca})₂] is very close to that in the structural formula of the corresponding samples (0.11 *versus* 0.10 for M236–116, 0.09 *versus* 0.09 for M236–098, and 0.12 *versus* 0.10 for 821–545; Table 6).

Average *M*^A–O bond lengths determined for both phases of the samples studied vary from 2.372 to 2.378 Å. They are slightly shorter than the Ca–O distance refined for a dolomite sample having an ideal composi-

TABLE 6. CRYSTAL DATA AND REFINED STRUCTURAL PARAMETERS FOR MONO- AND TWO-PHASE DOLOMITE, ANKERITE AND EXCESS-Ca DOLOMITE*

Parameters	Ankerite	M236-116, Ca _{1.10} Mg _{0.89} Fe _{0.01}		M236-098, Ca _{1.09} Mg _{0.91}		821-545, Ca _{1.10} Mg _{0.90}	
	Ca _{0.991} Mg _{0.676} Fe _{0.333}	Phase I	Phase II	Phase I	Phase II	Phase I	Phase II
<i>a</i> (Å)	4.8170(5)	4.8140(1)	4.8274(1)	4.8141(1)	4.8247(1)	4.8114(9)	4.8215(9)
<i>c</i> (Å)	16.0794(17)	16.0411(9)	16.1374(9)	16.0392(7)	16.1243(1)	16.025(3)	16.111(3)
<i>Z</i> _c	0.2430	0.2432(5)	0.2438(5)	0.2436(4)	0.2457(6)	0.2444(5)	0.2426(4)
<i>X</i> ₀	0.2502(1)	0.2520(5)	0.2505	0.2517(4)	0.2493(6)	0.2502(6)	0.2514(5)
<i>Y</i> ₀	-0.0329(4)	-0.0324(6)	-0.0338(6)	-0.0327(4)	-0.0344(7)	-0.0350(7)	0.0305(5)
<i>Z</i> ₀	0.2442(8)	0.2440(2)	0.2451(3)	0.2434(2)	0.2455(3)	0.2440(6)	0.2444(2)
<i>M</i> ^A –O(Å)	2.378(5)	2.372(3)	2.376(3)	2.378(4)	2.375(3)	2.378(2)	2.372(2)
<i>M</i> ^B –O(Å)	2.094(4)	2.087(3)	2.105(3)	2.084(3)	2.109(3)	2.081(2)	2.105(2)
<i>P</i> ^A _{Ca}	1.00	1.00	1.00	1.00	1.00	1.00	1.00
<i>P</i> ^A _{Mg}	0.00	0.00	0.00	0.00	0.00	0.00	0.00
<i>P</i> ^B _{Ca}	0.00	0.08(1)	0.17(1)	0.07(1)	0.13(1)	0.07(1)	0.14(1)
<i>P</i> ^B _{Mg}	0.67(1)	0.02(1)	0.83(1)	0.93(1)	0.87(1)	0.93(1)	0.86(1)
<i>P</i> ^B _{Fe}	0.33(1)	-	-	-	-	-	-
<i>B</i> ^A _{eq}	0.89(3)	0.89(3)	0.89(3)	0.84(3)	0.84(3)	0.96(3)	0.96(3)
<i>B</i> ^B _{eq}	0.90(3)	0.98(5)	0.98(5)	0.84(4)	0.84(4)	1.24(5)	1.25(5)
<i>B</i> ^{ns} _{eq}	0.94(4)	1.00(3)	1.00(3)	0.93(2)	0.93(2)	1.10(3)	1.10(3)
<i>W</i> (%)	100	52	48	62	38	40	60
<i>R</i> _{exp} (%)	3.86	2.56	2.56	2.61	2.61	2.59	2.59
<i>R</i> _{wp} (%)	5.24	6.24	6.24	5.86	5.86	6.87	6.87

*B*_{eq} = equivalent isotropic temperature-factor. * *A*, *B* and carbon sites are on special positions with the following coordinates: *A*(0, 0, 0); *B*(0, 0, ½), carbon (0, 0, *Z*_c).

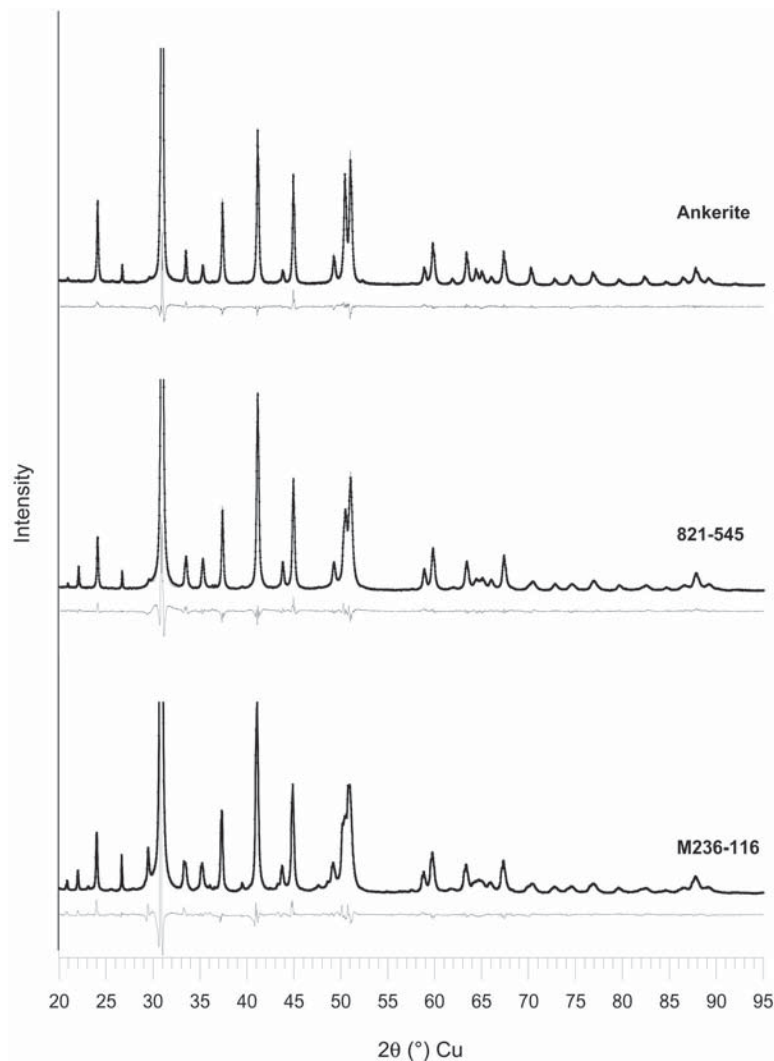
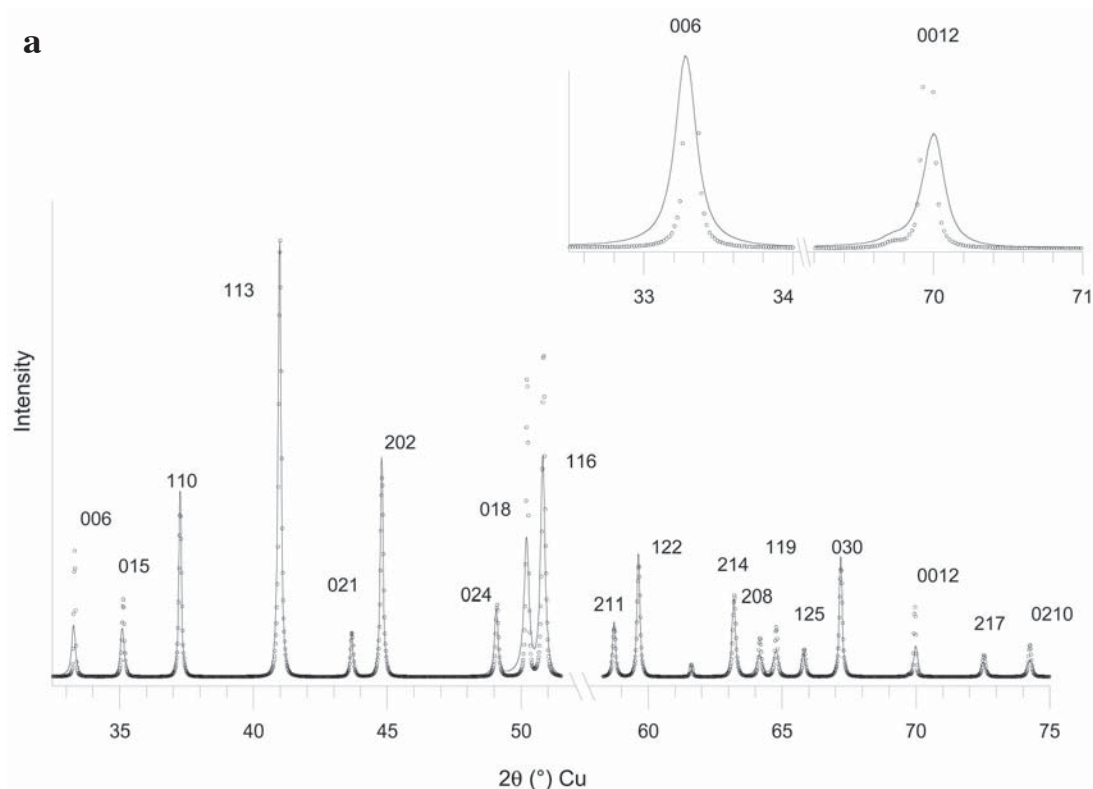


FIG. 4. Comparison of the experimental powder XRD patterns from ankerite, 821-545 and M236-116 samples with those obtained by the Rietveld refinements.

tion (2.380 Å; Reeder 1983). It is remarkable, however, that the M^A -O distances determined for phases I and II of the samples studied are very similar to each other, showing that the cation composition of the A sites in both phases is the same, and most probably these sites are occupied only by Ca (Table 6). Interatomic distances M^B -O in phase I are significantly shorter than those in phase II because the excess Ca in phase II is higher than in phase I. In particular, the M^B -O distances in phase I varies from 2.081 to 2.087 Å, whereas in phase II, they vary from 2.105 to 2.109 Å. However, the interatomic M^B -O bond lengths in both phases are underestimated approximately by 0.01–0.02 Å in comparison with those

expected if statistically weighted M^B -O distances were calculated for the cation compositions of the B sites, taking into account Ca-O = 2.38 Å and Mg-O = 2.084 Å, determined for ideal dolomite (Reeder 1983).

For example, the refined proportion of cations in phase II of sample M236-116 is $\text{Ca}_{1.13}\text{Mg}_{0.87}$ (Table 6) and, therefore, the expected (Mg,Ca)-O distances should be equal to 2.12 Å. The refined M^B -O value for this phase is 2.105 Å. However, one has to take into account that the mean Mg-O and Ca-O distances in the B octahedra of excess-Ca dolomite may differ from those determined for stoichiometric dolomite



(Reeder & Dollase 1989). At the same time, similar M^B -O distances determined for each of the phases of the samples studied show that the B sites of each phase have similar occupancy. This fact correlates with similar occupancies of the B sites in each phase determined by refinement (Table 6). Isotropic displacement parameters for the A , B and oxygen sites are much higher than those determined for stoichiometric dolomite (Reeder 1983). However, they are similar to those determined for ankerite (Table 6). Most probably, the isotropic displacement parameters result from the averaging of slightly different positions in the B layers owing to their complex composition.

DIFFRACTION FEATURES OF DIFFERENT DEFECTIVE-LAYER STRUCTURAL MODELS OF EXCESS-CA DOLOMITE

Qualitative analysis of the experimental XRD patterns shows that at least two of their features are associated with disturbance of the periodic and homogeneous structure of the samples. First, an increase of l values is accompanied by a significant increase in the broadening and attenuation of the hkl reflections. Second, results of the unit-cell refinements show that a noticeable difference between experimental and calcu-

lated d values is observed for reflections with a certain hkl . Most commonly, this difference is observed for $00l$ reflections. In order to understand, at least on the qualitative level, the origin of these diffraction features, different defective-layer models for excess-Ca dolomite have been considered. For each model, the powder XRD pattern has been calculated for the interval 19.0 – $75.0^\circ 2\theta$. Intensities were calculated with a step equal to $0.02^\circ 2\theta$. The thickness of coherent scattering domains (CSD) is considered to be distributed log-normally, and the parameters of this distribution were determined using the mean number of dolomite layers in CSD and the regression given by Drits *et al.* (1997), with mean (N) and maximum (N_{\max}) numbers of dolomite layers in CSD as variable parameters. For all models, $N_{\max} = 100$, and N values were varied from 60 to 100. The CSD were assumed to have a disc-like shape, with a diameter varying from 200 to 1200 Å.

To visualize the influence of each particular defect on the diffraction features, the XRD patterns of different models are compared with that calculated for an idealized defect-free structural model for excess-Ca dolomite. The unit-cell parameters in the model are a 4.822, c 16.123 Å. Cartesian coordinates for the 16.123 Å layer unit were taken from the Rietveld refinement of sample 821–545 (Table 6). The cation proportions

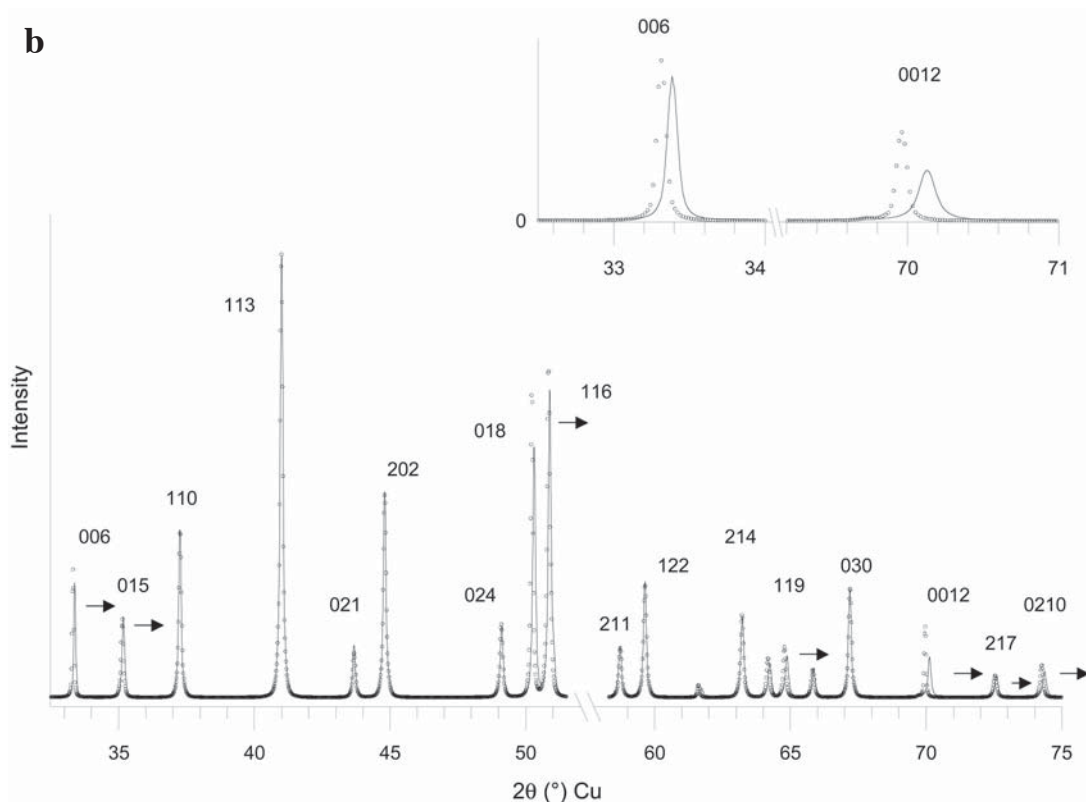


FIG. 5. Comparison of XRD patterns calculated for a periodic Ca-dolomite structure consisting of 16.123 Å layers (dotted line) with those calculated for (a) a mixed-layer excess-Ca dolomite – calcite model containing 96% of 16.123 Å dolomite and 4% of 17.06 Å calcite layers (solid line), and (b) a mixed-layer model in which 70% of 16.123 Å layers are interstratified with 30% of 16.008 Å stoichiometric dolomite layers (solid line) (for details, see Table 7).

at the *A* and *B* sites are equal to Ca_1 and $\text{Mg}_{0.86}\text{Ca}_{0.14}$, respectively. Intensities of the *hkl* reflections are calculated on the same scale, that is, XRD patterns from different models can be directly compared with each other. Structural and probability parameters describing the structural models used for the calculations are given in Table 7.

Interstratification of excess-Ca dolomite and calcite-like layers

In this model, 16.123 Å layers corresponding to the defect-free excess-Ca dolomite are interstratified with 17.06 Å calcite-like layers. The probability of occurrence of two adjacent calcite-like layers is equal to zero, that is, the short-range order factor *R* is equal to 1. Atom coordinates for the calcite-like layers were taken from the refined structure of calcite (Effenger *et al.* 1981). We assume that both types of layers have the same lateral dimensions (discussed below). Calculations

show that even a 1% excess of calcite-like layers significantly modifies the intensity distribution in comparison with that of a defect-free model. In Figure 5a, we compare the XRD patterns calculated for the periodic 16.123 Å structure and for the mixed-layer model containing 4% of calcite-like layers.

There is some general regularity in the intensity modifications relating to calcite-like layers. First, the presence of calcite-like layers is accompanied by significant attenuation of reflections having a particular *hkl*. The higher the *l*, the stronger the maximum intensity decreases. Second, a decrease in the intensities of the *hkl* reflections with *l* is accompanied by a broadening of the reflections. The higher the *l*, the broader is the reflection FWHM. Finally, the most significant effect of the interstratification is manifested by the behavior of basal reflections. They not only decrease in intensity and increase in width, but are shifted from the positions corresponding to those of the defect-free structure. The shift of these reflections is rather peculiar, because 006

and 0012 peaks are moved toward lower and higher 2θ angles, respectively (Fig. 5a).

Interstratification of layers having excess Ca and ideal dolomite compositions

Two limited cases are considered in which excess-Ca dolomite and ideal dolomite layers are interstratified. In one of them, 16.123 Å layers of the defect-free model prevail, whereas in the other, their proportion is reversed. The atom coordinates for the 16.008 Å ideal dolomite layer are taken from the refined structure of Reeder (1983). We assume that layers with a lower content of Ca adjust their lateral dimensions to those of the layers with the greater abundance. The XRD pattern shown in Figures 5b corresponds to the model containing 30% layers of stoichiometric dolomite. One can see that the main diffraction-effects from such mixed-layer structure is that hkl reflections (including $00l$ maxima) are shifted toward positions of hkl reflections corresponding to a stoichiometric dolomite. The higher the content of the latter layers, the higher the shift of hkl reflections. It is remarkable, however, that reflections having different hkl have different sensitivity to displacement from their position in the defect-free structure. As can be seen in Figure 5b, the higher the l , the larger shift of the hkl reflections.

Interstratification of excess-Ca dolomite and γ -dolomite structure layers

In this structural model, 16.123 Å layers are interstratified with 16.385 Å layers having the following sequence of cations along the c axis: CaMgCa-CaCaMgCa... . The content of γ layers varies from 2 to 15%, and the probability of occurrence of two adjacent γ layers is equal to zero. As can be seen in Figure 6a, an increase of the γ layers is accompanied by displacement of hkl reflections toward those corresponding to periodic γ structural models, that is, toward lower- 2θ angles. In addition, an increase of γ layers is accompanied by attenuation and broadening of hkl reflections with high l (Fig. 6a).

Fluctuations in layer thickness

Compositional heterogeneity, observed by TEM as modulations, intergrowths, or strain, may be associated with fluctuations in thickness of the dolomite layer, either if fragments of Ca-rich and Ca-poorer layers are interstratified or if a lateral distribution of Ca contents within the same layers is irregular. As a result, in the average structure of excess-Ca dolomite, layer thicknesses may vary about the mean value.

The mathematical formalism describing the intensity distribution in periodic and mixed-layer structures containing fluctuations in layer thickness distributed without long-range correlation among defects (Guinier

1964) has been deduced by Drits & Tchoubar (1990). In particular, in simulating the XRD patterns of layer structures, the distribution of the layer thickness is described by a normal Gaussian distribution of specific standard deviation, ΔH , for a given layer-type. If we assume that the thickness of the excess-Ca dolomite layer is $16.123 \text{ \AA} \pm \varepsilon$, where ε is a variable, then $\Delta H = (\overline{\varepsilon^2})^{1/2}$. The greater the ΔH , the larger the interval for variation of layer thickness.

Figure 6b shows XRD pattern calculated for a periodic excess-Ca dolomite structural model containing layer-thickness fluctuations with $\Delta H = 0.10 \text{ \AA}$. One can see that the presence of these defects dramatically modifies the intensity distribution of the reflection, by strongly decreasing intensities and increasing broadening of hkl reflections with l . These effects are especially strong for the 0012 peak. The characteristic redistribution of intensities of 018 and 116 reflections where $I(116) > I(018)$ are an indicator of the layer-thickness fluctuations in excess-Ca dolomite. It is important to note that the fluctuations change the intensities and widths of reflections, but not the positions of reflections.

Positional fluctuations in the ab plane

Compositional heterogeneity of excess-Ca dolomite may be also associated with a stack of layers in which the translation vector in the ab plane is subject to fluctuations that follow a Gaussian distribution without long-range correlation among the defects. A mathematical formalism describing position fluctuations was

TABLE 7. STRUCTURAL AND PROBABILITY PARAMETERS FOR THE STRUCTURAL MODELS OF EXCESS-Ca DOLOMITE USED IN THE CALCULATION OF THE POWDER-DIFFRACTION PATTERNS

Model A: B	Thickness of the layers		Proportion of the layers		a Å	ΔH Å	$\Delta t/a$
	h_A (Å)	h_B (Å)	w_A	w_B			
Excess-Ca dolomite – calcite	16.123	17.060	0.96	0.04	4.822	0	0
Excess-Ca dolomite – dolomite	16.123	16.008	0.7	0.3	4.822	0	0
Dolomite – excess-Ca dolomite	16.008	16.123	0.7	0.3	4.8077	0	0
Excess-Ca dolomite, fluctuations in layer thickness	16.123	-	1	0	4.822	0.10	0
Excess-Ca dolomite, positional fluctuations	16.068	-	1	0	4.818	0	0.03
Excess-Ca dolomite – γ -dolomite	16.123	16.385	0.85	0.15	4.822	0	0

Note: h_i and w_i are the thickness and probability of occurrence of the interstratified layers ($i = A, B$). For all models, $N = 80$, $L = 700 \text{ \AA}$.

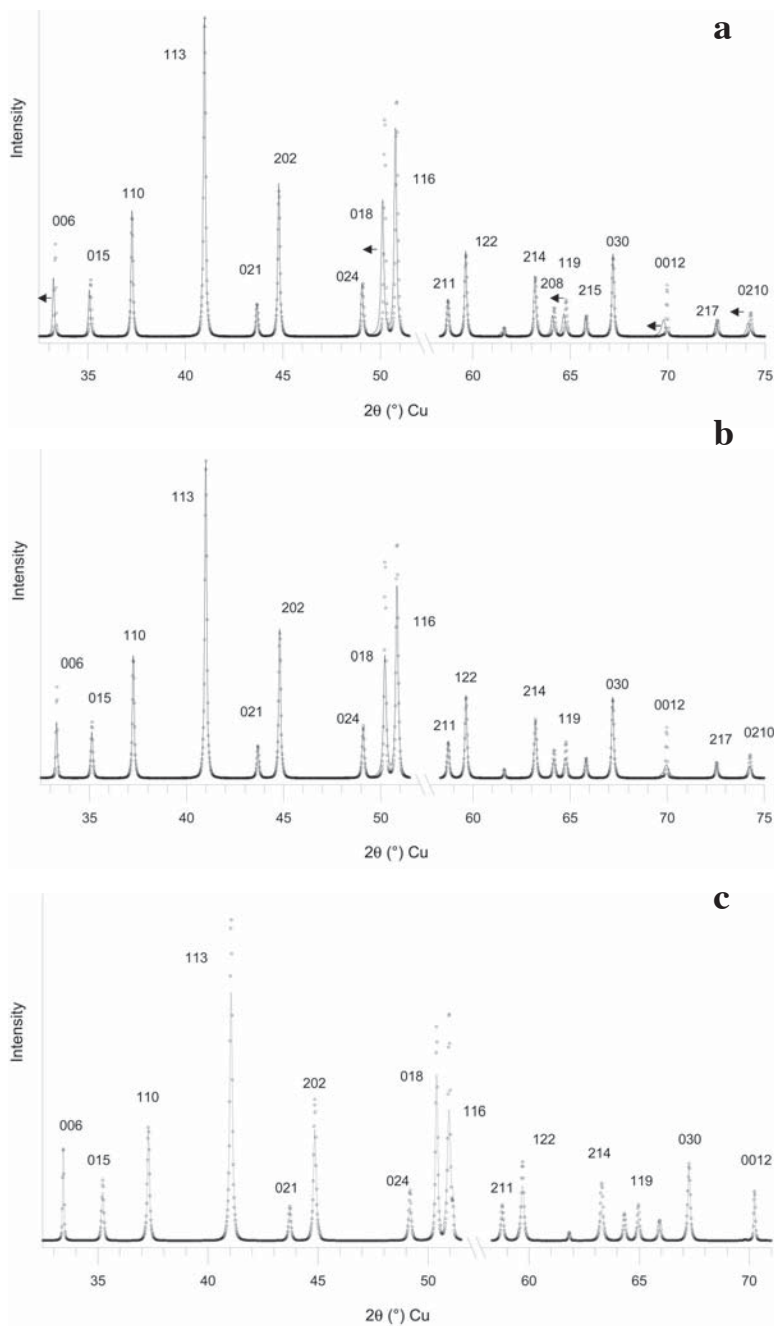


FIG. 6. Comparison of XRD patterns calculated for a periodic excess-Ca dolomite structure consisting of 16.123 Å layers (dotted line) with those calculated for models corresponding to (a) a mixed-layer structure in which 85% of 16.123 Å dolomite layers are interstratified with 15% of 16.385 Å layers, forming a γ -structure (solid line); (b) the periodic 16.123 Å excess-Ca dolomite model in which fluctuations of the layer thicknesses take place with $\Delta H = 0.10$ Å (solid line); (c) the periodic 16.123 Å excess-Ca dolomite model in which variation of the translations in the ab plane occur with $\Delta t/a = 0.03$ (solid line) (for details, see Table 7).

given in Drits & Tchoubar (1990). The XRD patterns in Figure 6c were calculated for a structural model in which positions of the 16.123 Å layers are varied with $\Delta t/a = 0.03$ around the mean translation in the *ab* plane that determines the ideal layer-stack. Here Δt has the same meaning as ΔH , but in the case of positional fluctuations in the *ab* plane, a variable ε describes a Gaussian distribution of interlayer translations. As can be seen in Figure 6c, the variation of translations within the *ab* plane leads to a decrease of intensities and an increase of broadening of *hkl* reflections. However, in contrast to the layer-thickness fluctuations, the positional variations do not disturb intensities of the 00*l* reflections.

*Simulation of XRD patterns
from various structural models*

In this section, we will simulate the powder XRD patterns of samples of excess-Ca dolomite, including not only basal but also *hkl* reflections. In such simulations, we base the analysis on the diffraction features observed in the experimental XRD patterns and also those calculated from the various structural models described above. We emphasize that our efforts are confined to the defects that disturb the periodic and homogeneous structure of dolomite and lead to symmetrical or asymmetrical broadening of *hkl* reflections, and also to their shifts from positions determined by the periodic lattice. Unfortunately, our approach has low sensitivity to the distribution of Ca and Mg cations over the *A* and *B* sites and to slight changes of the atom coordinates. For these reasons, we aspire primarily to obtain satisfactory agreement between shapes and positions of the calculated and experimental reflections. Below, the results of the simulation will be described for several samples in which phase, compositional, and structural heterogeneity are complicated.

Case 1: samples M214–034 and M236–104

At the outset, XRD patterns are calculated for the 3D periodic structures of excess-Ca dolomite using unit-cell parameters refined for each of the samples (Table 2). Comparison of these patterns to observed ones shows that a noticeable disagreement between calculated and experimental $d(hkl)$ and $2\theta(hkl)$ occurs for *hkl* reflections with high *l*.

This regularity is a characteristic feature of XRD patterns from mixed-layer excess-Ca dolomite – dolomite (Fig. 5b). However, for this model, both the 006 and 0012 should be shifted in the same direction toward higher 2θ angles if the content of the excess-Ca dolomite layers prevails. These displacements contradict the experimental positions of these reflections, which are shifted toward lower and higher 2θ angles, respectively, with respect to their positions describing the refined unit-cell (Table 2).

To compensate the “incorrect” shift of the 006 reflection along with layers of excess-Ca dolomite and ideal dolomite, the mixed-layer structure should contain a small proportion of calcite layers. These calcite layers provide a shift of the 006 reflection toward lower 2θ and for the 0012 reflection toward higher 2θ (Fig. 5a). Indeed, as can be seen in Figures 7a and 7b, in both samples interstratification of Ca-rich dolomite, stoichiometric dolomite, and calcite layers in the proportion 0.865:0.10:0.035 leads to a satisfactory agreement between the experimental and calculated positions and profiles of *hkl* reflections, including the basal ones. The thickness of layers of excess-Ca dolomite for samples M236–034 and M236–104 is equal to 16.034 and 16.047 Å, respectively. A significant increase of reflection-broadening with *l* observed in the experimental XRD patterns (Figs. 7a, b) along with the interstratification is provided by the layer-thickness fluctuations with a standard deviation ΔH of 0.095 Å and 0.11 Å for samples M214–034 and M236–104, respectively. In addition, the optimal mixed-layer models include positional variations of translations within the *ab* plane with a standard deviation $\Delta t/a = 0.02$ and 0.015, respectively. All parameters used for the simulation are given in Table 8.

Figure 7b includes an insert fragment of the calculated and experimental XRD patterns of sample M214–034 containing the strongest 104 reflections. Many essential details concerning correlation between the calculated and experimental positions and profiles of the much weaker *hkl* reflections are not seen properly. Agreement between the experimental and calculated XRD pattern is seen to be significantly better if the 104 reflection is excluded (Fig. 7b). Therefore, in the following examples of experimental and calculated XRD patterns, the 104 reflection will be artificially removed.

Case 2: sample 821–019

As can be seen in Figure 2a, the low- 2θ region of the XRD pattern contains direct evidence for the coexistence of two phases because the 006 and 015 reflections are split after the $K\alpha_2$ contribution was removed. The main diffraction feature of the experimental XRD pattern of sample 821–019 is that its high- 2θ region looks like that of a monophase sample (Fig. 2b).

This apparent contradiction is related to specific structural features of the coexisting phases. In one of them, 16.08 Å excess-Ca dolomite layers are interstratified with 17.06 Å calcite layers in a proportion 0.97:0.03, whereas the other model has 3D periodicity and consists of almost stoichiometric 16.022 Å dolomite layers. The presence of calcite layers in the mixed-layer phase provides a significant displacement of the 0012 reflection toward the higher 2θ angles. As a result, the 0012 reflections of both excess-Ca phases almost overlap, forming one rather wide maximum. For both

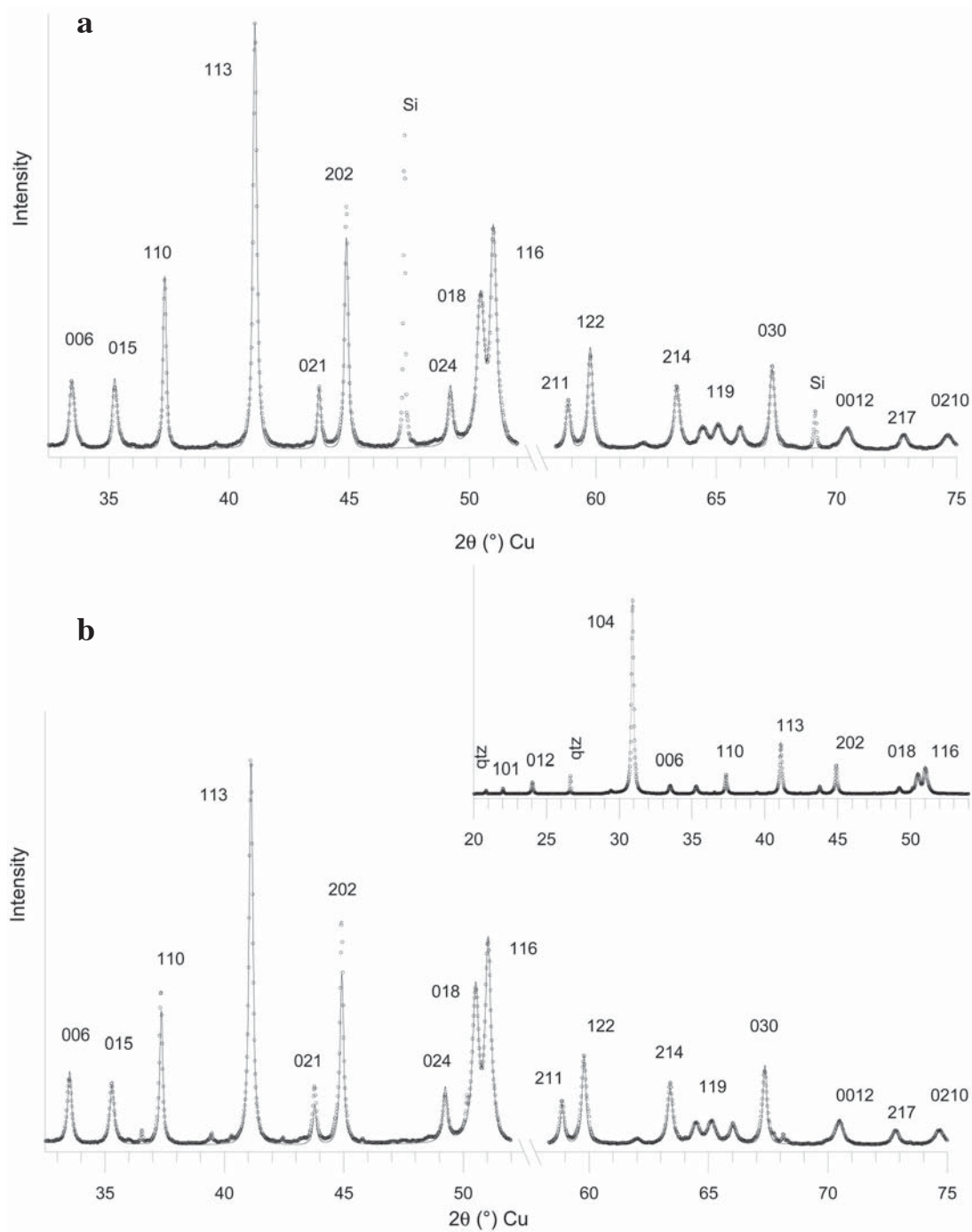


FIG. 7. Comparison of the experimental powder XRD patterns from samples M236-104 (a) and M214-034 (b) (dotted line) with those calculated for mixed-layer structural models (a) consisting of 86.5% of 16.047 Å excess-Ca dolomite, 10% of 15.99 Å stoichiometric dolomite and 3.5% of 17.06 Å calcite layers (solid line) and (b) consisting of 86.5% of 16.034 Å excess-Ca dolomite, 10% of 15.99 Å stoichiometric dolomite and 3.5% of 17.06 Å calcite layers (solid line) (for details, see Table 8). A fragment of the experimental and calculated powder XRD patterns containing the strongest reflection (104) is given in Figure 7b for sample M214-034.

phases, ΔH is equal to 0.07 Å, whereas $\Delta t/a$ is equal to 0 and 0.03 for the mixed-layer and periodic structures, respectively (Fig. 8a, Table 8).

Case 3: sample M236-081

Satisfactory agreement between the experimental and calculated XRD patterns is achieved for a three-phase model (Fig. 8b). One of them corresponds to a periodic excess-Ca dolomite structure with a 4.8266 Å, c 16.149 Å, ΔH 0.13 Å and $\Delta t/a$ 0.01. The other two mixed-layer phases contain 2% calcite layers each, and differ from each other by the thickness of the excess-Ca dolomite layers, equal to 16.07 and 16.02 Å, respectively. For the last two phases, $\Delta t/a$ and ΔH are equal to 0.02 and 0.09 Å, and 0.01 and 0.08 Å, respectively (Table 8).

Scanning electron microscopy (SEM)

SEM images obtained for the two-phase samples show that their common feature is the coexistence in each sample of two populations of crystals having distinctly different sizes. For example, Figure 9a shows large crystals surrounded by a mass of very small crystals of dolomite (micrite). Under higher magnification (Fig. 9b), the micrite consists of microcrystals of irregular shape, whereas the large crystals abut open

macroporosity and have prominently euhedral forms intergrown into adjacent crystals. Such features are also observed for samples M236-116, M236-098, M236-081, and M236-073. Similar, but not identical, SEM images were observed for samples 821-546, 821-545, and 821-549 (e.g., Figs. 9c, d). For these samples, large crystals of excess-Ca dolomite prevail, and their rhombic shape is perfectly expressed.

Back-scattered electron (BSE) images and electron-microprobe analysis

On the basis of SEM images, it seemed natural to assume that, given their coexistence in the same sample, the two excess-Ca dolomite phases and the two size populations of crystals would correspond. Therefore, the initial task of the BSE analysis was to determine the difference in Ca-content of the large and small crystals of dolomite and to determine which of the two populations has the higher Ca-content. Results obtained by electron-microprobe analysis show, however, that there is no relationship between excess in Ca uptake and size. Figure 10 shows that within single crystals of both large and small size, there are dark and light zones that correspond to differing Ca:Mg ratios.

A distinct feature of the two-phase samples is that most of them are almost (Fe + Mn)-free. We found, however, that a few coarse crystals in sample M236-116

TABLE 8. STRUCTURAL AND PROBABILITY PARAMETERS USED FOR SIMULATION OF THE EXPERIMENTAL POWDER-DIFFRACTION PATTERNS OF THE SAMPLES OF DOLOMITE STUDIED

A	B	C	Thickness of layers			Proportion of the types of layers			a Å	ΔH Å	$\Delta t/a$	\bar{N}	L Å ***	$N(\alpha)$ *	K % **
			h_A Å	h_B Å	h_C Å	W_A	W_B	W_C							
XsCa dol : Dol : Cal (M214-034)			16.034	15.99	17.06	0.865	0.10	0.035	4.8133	0.095	0.02	60	500	95	100
XsCa dol : Dol : Cal (M236-104)			16.0475	15.99	17.06	0.865	0.10	0.035	4.8138	0.11	0.015	35	500	110	100
XsCal dol : Cal			16.08	-	17.06	0.97	-	0.03	4.816	0.07	0	60	600	120	15
XsCa dol (M821-019)			16.022	-	-	1	-	-	4.812	0.07	0.03	20	600	120	85
XsCa dol			16.149	-	-	1	-	-	4.8266	0.13	0.01	40	550	120	49
XsCa dol : Cal			16.07	-	17.06	0.98	-	0.02	4.8134	0.09	0.02	40	500	120	27
XsCa dol : Cal (M236-081)			16.02	-	17.06	0.98	-	0.02	4.8134	0.08	0.01	40	500	120	24

* $N(\alpha)$: parameter of the normal distribution of the partial orientation function.

** K : relative weighted concentration of the various phases.

*** The mean size of coherent scattering domains in the ab plane was reduced to 100 Å for calculations of the 030 reflection because of strain within the layers of dolomite decrease the effective CSD for indices with high $h^2 + k^2$.

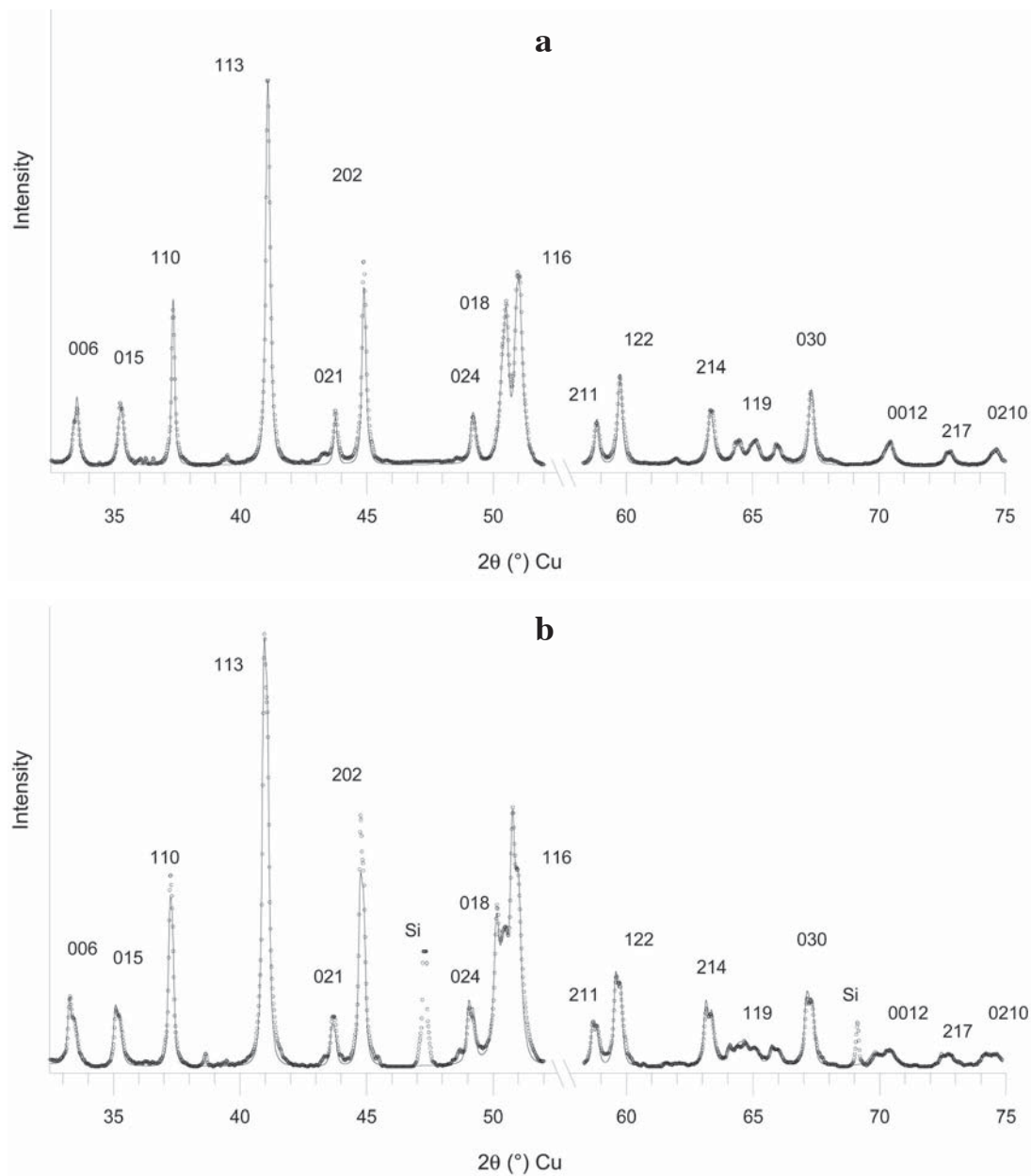


FIG. 8. Comparison of the experimental powder XRD patterns from samples, 821-019 (a) and M236-081 (b) (dotted line) with those calculated for (a) a physical mixture of two phases one of each has 3D periodicity and consists of 16.022 Å layers, whereas the other one has a mixed-layer structure in which 97% of 16.08 Å excess-Ca dolomite and 3.0% of 17.06 Å calcite layers are interstratified (solid line); (b) a three-component mixture consisting of a periodic 16.149 Å excess-Ca dolomite structure and two mixed-layer phases, each of which contains 2% of calcite layers and differs from each other by the layer thickness equal to 16.070 Å for one and 16.020 Å for the other mixed-layer phases (solid line).

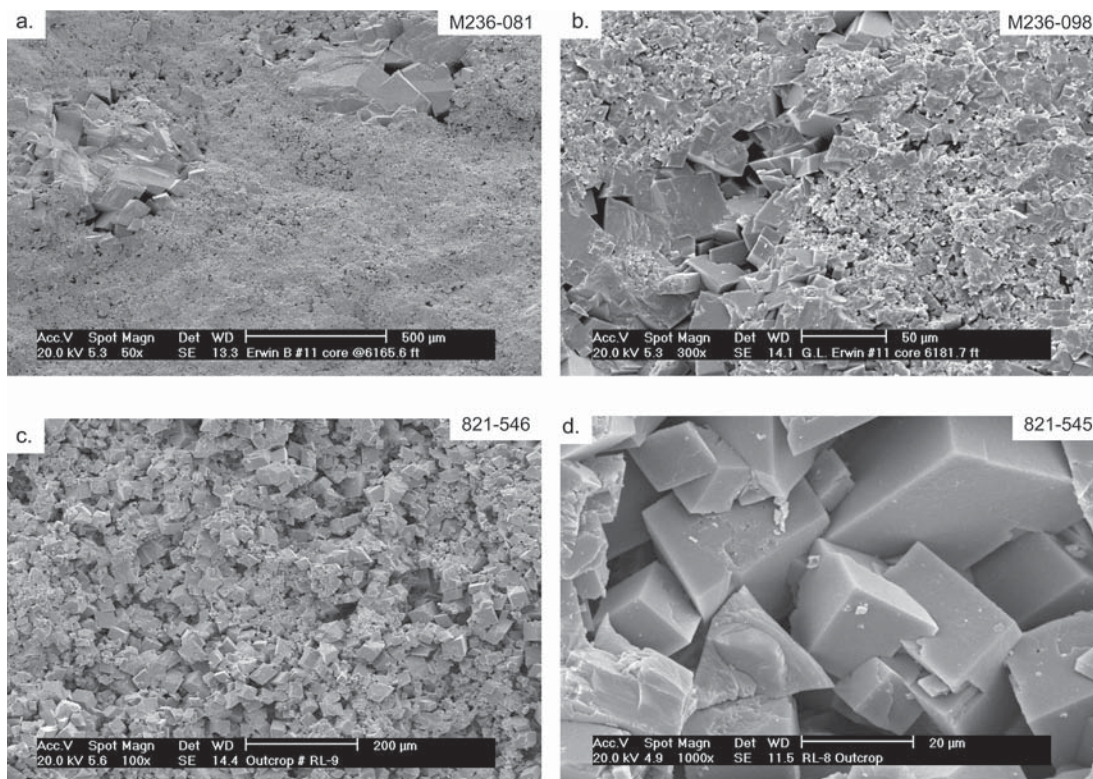


FIG. 9. Representative scanning electron microscope images demonstrating coexisting large euhedral and micritic excess-Ca dolomite crystals (for details, see the text).

contain 0.02–0.04 atoms of Fe per formula unit, and the BSE brightness of the corresponding spots increases accordingly. Therefore, although BSE brightness in these samples is largely a function of Mg:Ca ratio, Fe-rich zones complicate this trend locally. Given the complexity of multi-element control on relative BSE brightness, we undertook to compare cation compositions of different zones quantitatively.

Measurements of the levels of Ca, Mg, Fe, Mn and Sr were made at three to four different spots within individual zones, as observed in BSE (Table 9). Note that the experimental errors in the determination of amounts of Ca and Mg do not exceed 0.005 *apfu*, and variations in amount of Ca relative to the mean value within individual zones seldom exceed this value (Table 9). Therefore, we conclude that each particular zone has a homogeneous composition, within the precision of the determination. Analysis of the amounts of Ca in zones having different intensity of BSE shows that in sample M236–116, there are four non-overlapping groups differing in their Ca and Mg contents (zones 1–4, 5, 6–7, 8–9; Table 9). The mean values of the Ca contents within each group, along with the deviations about these means, are equal to (1.066 ± 0.004) , $(1.092$

$\pm 0.004)$, (1.106 ± 0.006) and (1.130 ± 0.001) , respectively (Table 10).

A similar conclusion is valid for sample M236–081, for which four compositional zones also can be distinguished (zones 2–3, 4–5, 6–7, and 8; Table 9). The mean amounts of Ca and the mean deviations are given in Table 10. For sample M236–098, some zones have wider intervals of variation of Ca and Mg (zones 5–7, Table 9). Taking into account the width of the probe beam ($\sim 10 \mu\text{m}$) and the depth of its penetration into the sample ($\sim 10 \mu\text{m}$), we can infer that each particular measurement corresponds to a volume that is large relative to the finest zones seen in BSE. Therefore, it is not surprising that one or two domains in which the difference in amounts of Ca and Mg is about 0.01–0.02 *apfu* may coexist within a zone having almost the same BSE intensity. However, in order to detect a possible preferential occurrence of Ca and Mg contents, we are interested to establish compositions at each measured spot. In this case, for sample M236–098, three groups of zones and domains differing in Ca content can be distinguished (Tables 9, 10).

The micritic dolomite in samples M236–116 and M236–098, like their coarser counterparts, consists of

distinct compositional fields (Table 9) corresponding to BSE brightness. It is notable that the average amounts of Ca *in apfu* determined for these fields are almost identical to those determined for the coarse crystals of the same samples (Table 10).

TABLE 9. CONTENTS OF Ca, Mg AND (Fe + Mn + Sr) IN VARIOUS ZONES OF THE SAMPLES STUDIED

Zone	Ca	Mg	Fe + Mn + Sr	Zone	Ca	Mg	Fe + Mn + Sr
Sample M236-116, coarse crystals							
1	1.060	0.938	0.002	6	1.108	0.890	0.0014
	1.066	0.932	0.0018		1.112	0.886	0.0012
	1.066	0.932	0.0042		1.110	0.888	0.0014
2	1.072	0.924	0.0044	7	1.100	0.852	0.0482
	1.060	0.938	0.0032		1.102	0.850	0.0480
	1.056	0.938	0.0048		1.106	0.844	0.0506
3	1.066	0.930	0.0050	8	1.122	0.876	0.0014
	1.070	0.930	0.0044		1.130	0.868	0.0020
	1.066	0.932	0.0134		1.134	0.864	0.0012
4	1.074	0.926	-	9	1.134	0.866	0.0008
	1.070	0.928	0.0014		1.138	0.862	0.0002
	1.058	0.940	0.0024		1.132	0.868	0.0002
5	1.098	0.886	0.0150	10	1.070	0.930	0.0008
	1.090	0.894	0.0166		1.084	0.916	0.0006
	1.088	0.896	0.0172		1.080	0.918	0.0034
Sample M236-081, coarse crystals							
1	1.030	0.968	0.0010	5	1.040	0.956	0.0054
	1.020	0.980	0.0006		1.050	0.944	0.0052
	1.004	0.996	0.0004		1.048	0.946	0.0050
2	1.008	0.992	0.0004	6	1.066	0.932	0.0052
	1.012	0.988	0.0000		1.070	0.930	0.0008
					1.066	0.936	0.0004
3	1.004	0.992	0.0036	7	1.070	0.930	0.0000
	1.004	0.994	0.0004		1.062	0.932	0.0054
	1.000	0.998	0.0002		1.066	0.934	0.0000
4	1.052	0.930	0.0172	8	1.116	0.882	0.0012
	1.048	0.934	0.0166		1.116	0.882	0.0008
	1.040	0.928	0.0220		1.114	0.894	0.0012
Sample M236-098, coarse crystals							
1	1.054	0.946	0.0004	5	1.096	0.904	0.0002
	1.052	0.948	0.0002		1.096	0.904	0.0002
	1.044	0.956	0.0002		1.094	0.906	0.0008
	1.040	0.960	0.0020		1.116	0.884	0.0006
2	1.056	0.944	0.0004	6	1.102	0.898	0.0008
	1.052	0.946	0.0012		1.098	0.900	0.0006
	1.066	0.936	0.0008		1.114	0.886	0.0002
					1.120	0.880	0.0008
3	1.054	0.924	0.0236	7	1.116	0.882	0.0006
	1.054	0.92	0.0262		1.098	0.902	0.0008
	1.058	0.902	0.0394				
4	1.056	0.944	0.0002				
	1.038	0.960	0.0010				
	1.066	0.936	0.0008				
	1.058	0.942	0.0004				
	1.098	0.902	0.0004				

DISCUSSION

Ca-Mg order in excess-Ca dolomite having periodic structure

Determination of cation proportions in the A and B layers, even in an average unit-cell of excess-Ca dolomite, may provide important information about the energetic state of this mineral (Chai *et al.* 1995), as

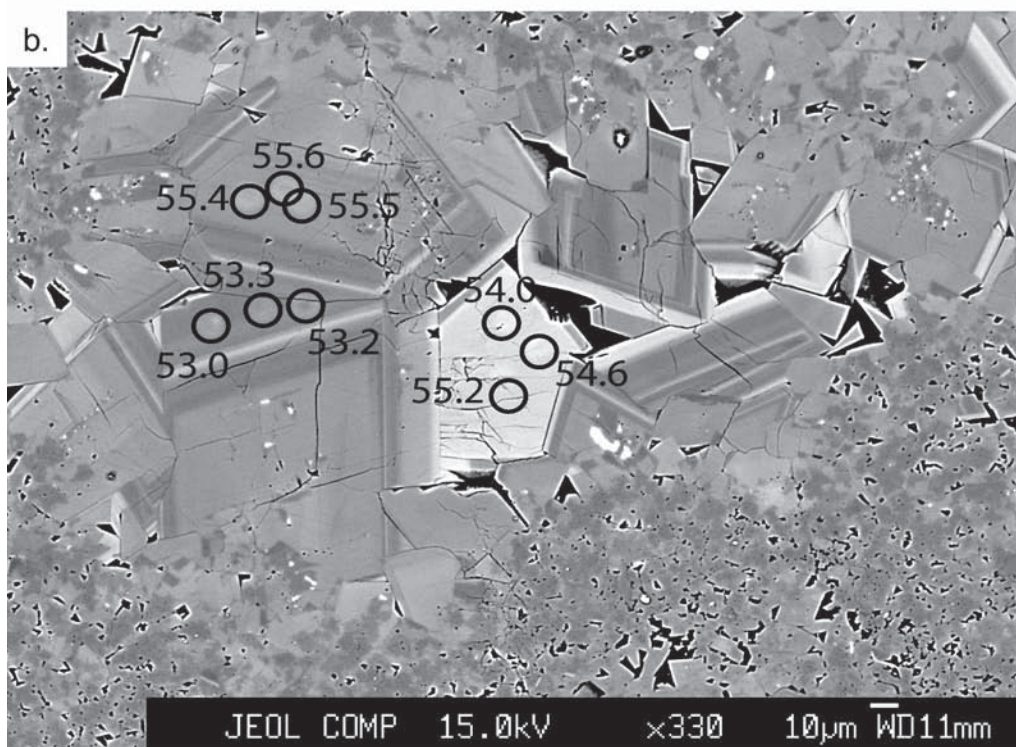
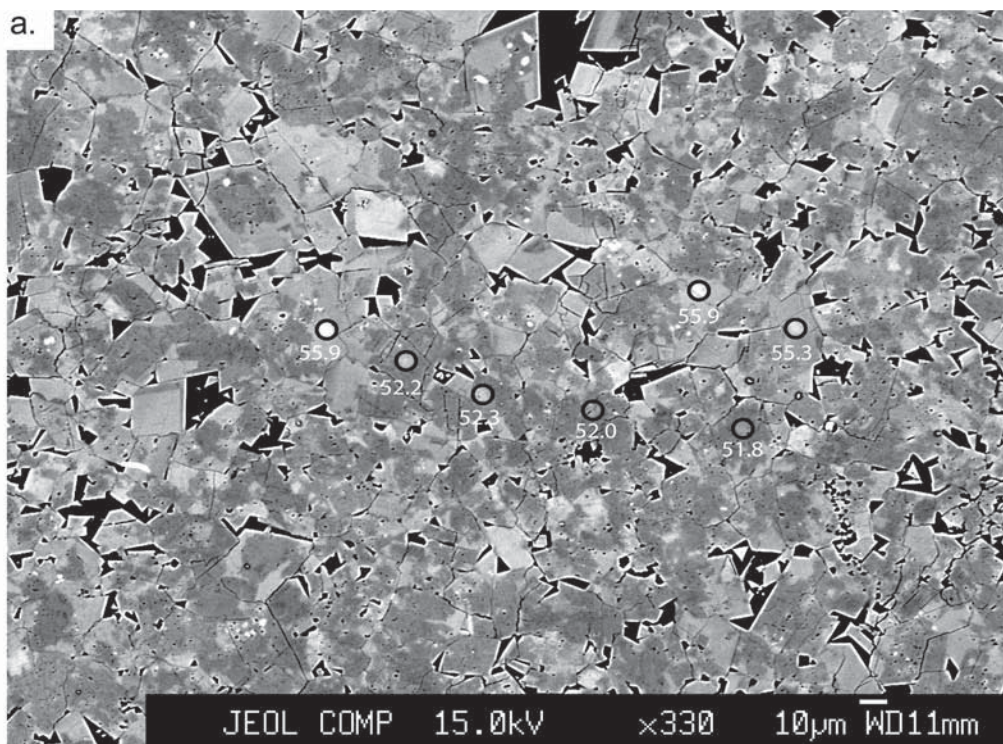
TABLE 9. CONTENTS OF Ca, Mg AND (Fe + Mn + Sr) IN VARIOUS ZONES OF THE SAMPLES STUDIED

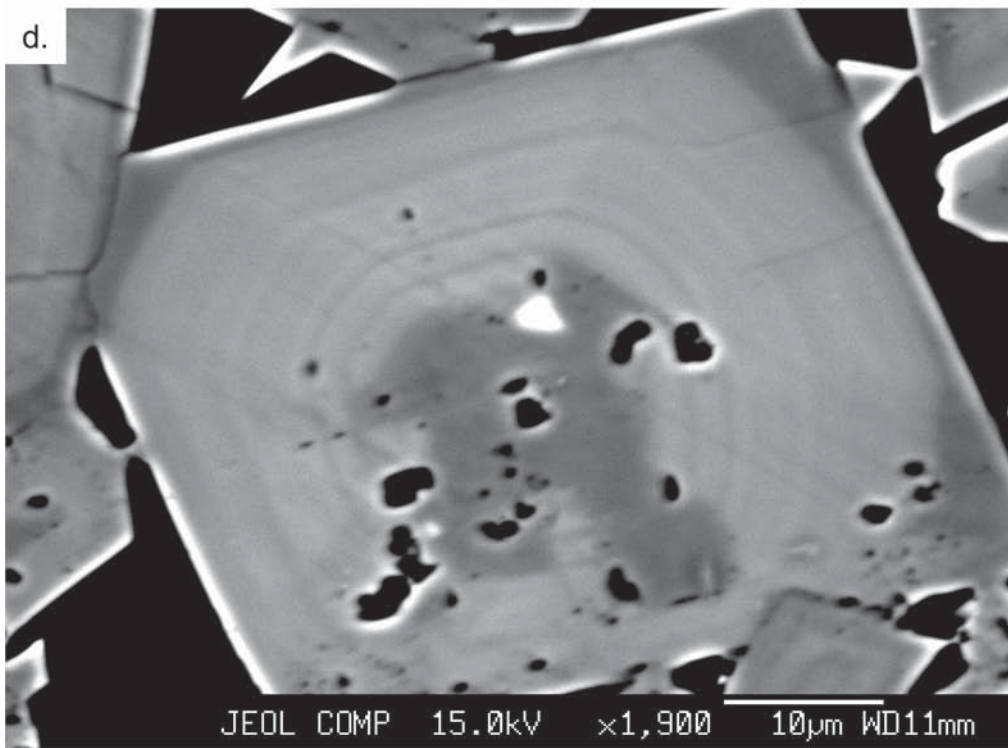
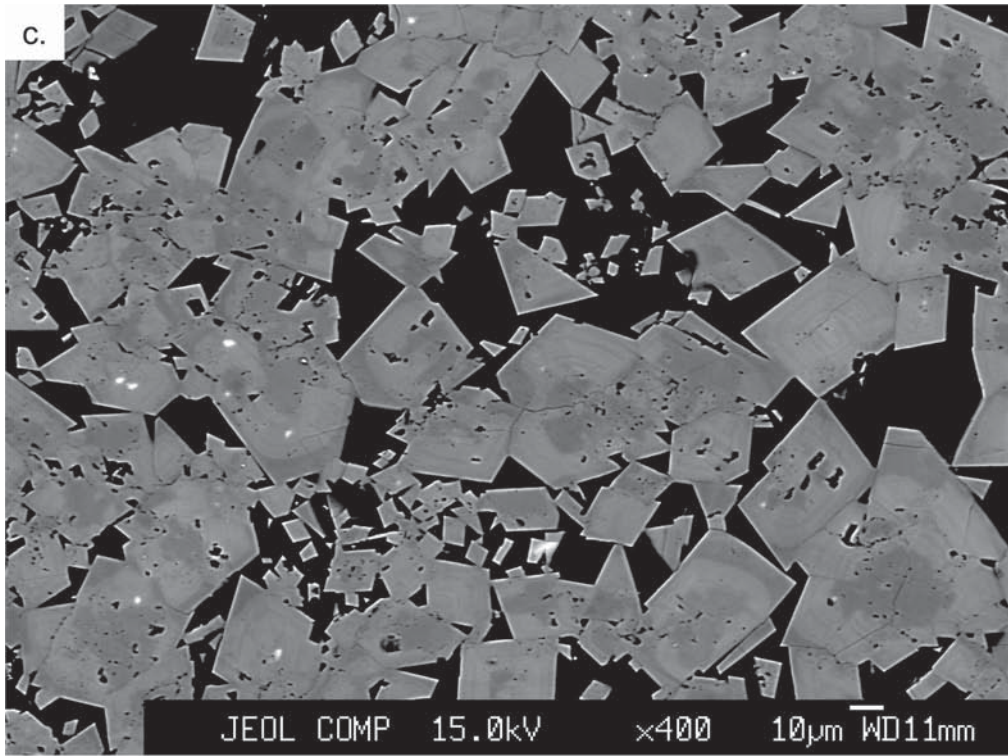
Zone	Ca	Mg	Fe + Mn + Sr	Zone	Ca	Mg	Fe + Mn + Sr
Sample 545, coarse crystals							
1	1.036	0.964	0.0008	3	1.088	0.910	0.0014
	1.030	0.968	0.0018		1.080	0.918	0.0012
2	1.070	0.928	0.0010		1.090	0.908	0.0004
	1.060	0.940	0.0002		1.088	0.912	0.0006
Sample M236-098, micrites							
1	1.044	0.954	0.0006	3	1.106	0.894	0.0002
	1.046	0.956	0.0008		1.118	0.882	0.0012
	1.040	0.958	0.0016		1.118	0.882	0.0004
	1.036	0.964	0.0000				
2	1.038	0.958	0.0044	4	1.118	0.882	0.0004
	1.046	0.950	0.0042		1.118	0.882	0.0006
	1.042	0.958	0.0008		1.096	0.904	0.0008
	1.044	0.956	0.0002		1.126	0.872	0.0008
Sample M236-116, micrites							
1	1.068	0.930	0.0024	4	1.098	0.900	0.0030
	1.072	0.946	0.0024		1.136	0.864	0.0000
	1.060	0.936	0.0040		1.134	0.866	0.0006
2	1.076	0.922	0.0018	5	1.120	0.878	0.0018
	1.074	0.924	0.0018		1.126	0.872	0.0018
	1.060	0.938	0.0024		1.126	0.872	0.0008
3	1.070	0.924	0.0052				
	1.066	0.930	0.0044				
	1.066	0.932	0.0038				
	1.084	0.914	0.0032				
	1.084	0.912	0.0038				

TABLE 10. THE AVERAGE AMOUNTS OF Ca IN DOLOMITE AND INTERVALS IN Ca CONTENT, WITH VARIATIONS ABOUT THE MEAN

Coarse crystals					
M236-116	-	1.066±0.006	1.092±0.004	1.106±0.004	1.130±0.001
M236-081	1.046±0.004	1.066±0.004	-	1.108±0.004	-
M236-098	1.050±0.006	-	1.098±0.004	1.116±0.002	-
Micrites					
M236-116	-	1.068±0.004	1.088±0.006	-	1.128±0.006
M236-098	1.042±0.004	-	-	1.116±0.004	-

The amount of Ca is expressed in atoms per formula unit (*apfu*).





well as provide constraints on models for the coexisting domains (Reeder 2000).

Surprisingly, in our collection of excess-Ca dolomite samples, none of the monomineralic samples has a 3D periodic structure suitable for Rietveld refinement. Therefore, we have used this method to refine structural parameters only for samples consisting of two ordered phases.

The low values of R_{wp} obtained for the samples studied (Table 6) confirm the 3D periodicity of the average structure of each coexisting phase. In these samples, *hkl* reflections do obey Bragg's law, and their profiles are well reproduced in simulated XRD patterns (Fig. 4). The main result obtained from the Rietveld refinements is that in both phases present in each sample, only *B* sites have a mixed population of Ca and Mg, whereas the *A* sites, with a high probability, contain only Ca. Thus, the main difference between phases I and II is that their *B* sites differ in their contents of Ca. We stress that the refined samples came from two quite different geological settings. Our results contrast with those of Reeder (2000) in that he found a mixed population of cations for both *A* and *B* sites in the two excess-Ca dolomite single crystals he studied. He found that the *A* and *B* sites consist of $\text{Ca}_{0.87}\text{Mg}_{0.13}$ and $\text{Mg}_{0.78}\text{Ca}_{0.22}$ for one of the crystal studied (sample 124–9B), and $\text{Ca}_{0.93}\text{Mg}_{0.07}$ and $\text{Mg}_{0.81}\text{Ca}_{0.19}$ for the other one (sample 124–23B).

We believe that the Ca–Mg order determined by the Rietveld technique corresponds to the actual average occupancy of the *A* and *B* layers for the following reasons. First, during refinement procedure, no constraints were implied for the composition of the *A* sites, and nevertheless the results invariably show that these sites are Mg-free.

Second, identical (within errors) $M^A\text{--O}$ distances determined in both phases of the samples studied indicate the same cation-occupancy of the *A* sites, whereas the mean value of these distances ($2.375 \pm 0.003 \text{ \AA}$) shows that these sites are essentially filled by Ca (Table 6). The systematic slight decrease of the refined $M^A\text{--O}$ bond lengths, in comparison with 2.380 \AA distance determined for ideal dolomite, most probably has the same explanation as that providing an increase of Ca–O

mean distance in ideal dolomite compared with the mean Ca–O = 2.36 \AA in calcite. There is also a decrease in the mean Ca–O bond length with increasing extent of Fe substitution at the *B* sites of ankerite (Reeder & Dollase 1989). According to these authors, the decrease of $M^A\text{--O}$ with Fe^{2+} at the *B* sites in ankerite is a consequence of the linkage of Ca-octahedra *via* corner sharing with (Mg, Fe) octahedra and CO_3 groups. As a result, the larger the (Mg, Fe) octahedra in ankerite, the smaller the mean Ca–O distances in the *A* layers. Similarly, an increase of the (Mg, Ca) octahedra in the *B* layers of excess-Ca dolomite is accompanied by the slight decrease of $M^A\text{--O}$ distances in comparison with 2.38 \AA in ideal dolomite (Table 6). In the limiting case in which the *B* layers are essentially filled by Ca, the mean length of the Ca–O bond decreases down to 2.36 \AA .

Third, it is likely that the different contents of Ca and Mg in the *A* and *B* layers in excess-Ca dolomite exert different patterns of influence on expansion of the *a* and *c* parameters. In particular, for all samples studied, the same regularity is observed: an increase in excess Ca uptake in dolomite is accompanied by a parallel increase in the *a* and *c* parameters. In particular, this effect is observed for the coexisting phases I and II: the *a* and *c* parameters of phase II are invariably larger than those of phase I (Table 3). It is logical to assume that an increase of Ca content in the *B* sites increases mean size of (Mg,Ca)-octahedra and, as a result, the unit cell expands along both the *a* and *c* axis.

This conclusion is in agreement with the evaluation of the *a* and *c* unit-cell parameters of ankerite samples of different composition studied by Reeder & Dollase (1989). In the ankerite structure, Fe substitutes for Mg at the *B* site and increases the mean size of (Fe,Mg) octahedra, which results in a linear increase of both the *a* and *c* unit-cell parameters. Similarly, in each phase of our refined two-phase samples, Ca substitutes for Mg at the *B* site, which should lead to a linear increase in the *a* and *b* parameters. For each phase, the following equations should be valid:

$$a = 4.8078 + K_1 \Delta n_{\text{Ca}}, \quad c = 16.0048 + K_2 \Delta n_{\text{Ca}}$$

where 4.8078 and 16.0048 \AA are the *a* and *c* parameters of the almost stoichiometric samples of Eugui dolomite (Antao *et al.* 2004), K_1 and K_2 are constants, and Δn_{Ca} is the excess Ca. In this case, a value of $\Delta a/\Delta c = (a - 4.8078)/(c - 16.0048)$ should be, within error, the same, independent of the Ca excess of the phases. Indeed, using unit-cell parameters for the high and low excess-Ca varieties of samples M236–116, 821–545, and M236–098, one can show that for all of them the $\Delta a/\Delta c$ ratio is equal to 0.133 ± 0.008 .

In contrast, according to Reeder (2000), a mixed proportion of cations in both *A* and *B* octahedra disturbs this regularity. For example, his excess-Ca dolomite (sample 124–23B), having a higher excess

FIG. 10. BSE images of dolomite crystals reveal compositional heterogeneities related to variations in Ca and Mg concentration. The same range of BSE contrast is observed within crystals of all sizes, microcrystalline (a, from sample M236–098) to coarse (b, from M236–116). Microprobe values of mole % CaCO_3 are shown on the images. In general, in larger crystals, compositional zones parallel the crystal boundaries. Images c and d (from sample 821–545) are examples of concentric zonation in single crystals of dolomite, again due to variations in proportions of Ca and Mg (see text for details). Small bright inclusions are calcite.

of Ca ($\text{Ca}_{1.12}\text{Mg}_{0.88}$), has a smaller a (4.8122 Å) and higher c (16.120 Å) parameters in comparison with those (4.8201 and 16.0721 Å) in sample 124–9B, with a lower total content of Ca ($\text{Ca}_{1.09}\text{Mg}_{0.91}$). Note that the occupancy of the B octahedra in samples 124–23B and 124–9B are similar ($\text{Ca}_{0.19}\text{Mg}_{0.81}$ and $\text{Ca}_{0.22}\text{Mg}_{0.78}$). The differing occupancy of the A octahedra thus has a decisive influence on particular changes of the unit-cell parameters in these samples. The relatively high content of Mg at the A sites of sample 124–9B ($\text{Ca}_{0.87}\text{Mg}_{0.13}$) in comparison with that in the A sites of sample 124–23B ($\text{Ca}_{0.93}\text{Mg}_{0.07}$) probably favors such an adjustment in the A and B layers, which is accompanied by their thinning at the expense of the increase in their lateral dimensions. In contrast, if only B layers had a mixed Mg–Ca occupancy, then the a and c parameters in sample 124–23B should be greater than those in sample 124–9B, in accordance with the total excess of Ca in these samples.

A comparison of the unit-cell parameters of excess-Ca dolomite studied by Reeder and in the present work (Table 3) shows that they do have quite different relationships between the a and c parameters. For example, phase I of samples M236–098 and 124–23B have similar a parameters (4.8134 versus 4.8122 Å), but quite different c parameters (16.0514 versus 16.120 Å). Similarly, phase II of samples M236–098 and 124–23B have similar c (16.136 versus 16.120 Å), but quite different a (4.8257 versus 4.8122 Å) parameters. Samples M214–034 and 124–23B have very similar a parameters (4.8133 versus 4.8122 Å), but quite different c parameters (16.034 versus 16.120 Å), and the cation distributions in the unit cell ($\text{Ca}_{1.06}\text{Mg}_{0.94}$ versus $\text{Ca}_{1.12}\text{Mg}_{0.88}$). All these observations show that the samples compared do differ in their occupancies of the A and B layers, confirming the conclusion that mixed occupancy occurs only in the B layers in our samples.

The location of the excess-Ca in the B layers is consistent with the SAED and TEM observations because both c and d types of domains having γ and δ structures provide extra Ca content only at the B site of the average unit-cell. In contrast, interpretation of a mixed-cation occupancy in both A and B sites of the average unit-cell requires some additional assumptions concerning the domain structure of dolomite (Reeder 2000).

Compositional heterogeneity and zonation in crystals of excess-Ca dolomite

The coexistence of growth zones of contrasting Ca-contents within dolomite single crystals, as seen in BSE images, suggests a complex history of formation and recrystallization. However, the origin of this intriguing phenomenon still remains poorly understood. What factors are responsible for the formation of zones differing in Ca:Mg ratio? Why are these zones separated from each other by sharp boundaries? Why does phase

II, having higher excess of Ca, as a rule, show a higher degree of structural order than that of phase I with a lower level Ca? What is the origin of compositional heterogeneity within zones corresponding to phases I and II? Why do compositions of zones corresponding to phases I and II, in the same sample, display almost the same compositional range for coarse-grained and fine-grained crystals of excess-Ca dolomite?

It has been generally accepted that the Ca/Mg value depends upon fluid composition, temperature, rock:fluid ratio, and structural and chemical transformations in the dolomite, in a general scheme according to which samples initially formed with significant excess of Ca, then recrystallized through a series of intermediate compositions to stable stoichiometric dolomite. Searl (1994) showed, however, that the rarity of continuous compositional gradients as opposed to sharply bounded growth-zones within dolomite crystals having compositional domains means that during growth only certain compositions form and, thus, solid solution within dolomite minerals is discontinuous. According to Searl (1994), Ca cations in the B layers are distributed regularly, forming seven discrete hexagonal unit-cells. Each of these cells reflects a certain amount of Ca uptake into the dolomite structure. Consequently, compositional zones have sharp boundaries because each zone can contain only a certain excess of Ca to provide for their regular distribution.

Such a model of discontinuous solid-solution in dolomite also suggests a structural control by which the composition of the preceding layer may to some degree determine the composition of the following one. Thus, the different compositions of coexistent zones in excess-Ca dolomite may depend not only on fluid composition, temperature and composition of the solid phase, but also on some crystal-chemical constraints on the variability of zone composition. This assumption is in agreement with conclusions of Fouke & Reeder (1992), that the Ca content in excess-Ca dolomite is at least partly controlled by surface structure and the growth mechanism, and is not in equilibrium with, or is not controlled by, the total content of Ca and Mg in the fluid.

Up to now, there is no direct evidence confirming the structural models of Ca and Mg order in excess-Ca dolomite proposed by Searl (1994). Numerous SAED patterns contain only the d - and c -type extra reflections described above. Nevertheless, many aspects of the discontinuous solid-solution model are reasonable from a crystal-chemical point of view and in agreement with many empirical observations. In particular, in the samples studied, the compositional zones of the coarse and fine dispersed fractions contain discrete sets of Ca content (Table 10), and this finding is consistent with the assumption that a growing crystal can have only certain compositions. The idea is that the ordered distribution of Ca in the B layers should increase the stability of the phase because it minimizes strains resulting from

substitution of the large Ca for the small Mg in the structure. Indeed, random distribution of Ca atoms and their segregation in clusters should create local sources of strain. In contrast, an ordered distribution of Ca and Mg should favor the formation of 3D periodic crystal lattices. These considerations are also in agreement with our observations on the structural order of phases I and II.

As was mentioned, phase II has a higher excess of Ca, and its structure is commonly described by a periodic 3D lattice. Growth of this phase thus took place under rather strong structural control that probably resulted not only because of the ordered distribution of Ca in the *B* layers, but also because of the rather high density of Ca uptake. In contrast, structural order of phase I having lower excess Ca uptake varies from sample to sample. One of the possible explanations is that at a low level of Ca uptake, there is a high dispersion of these cations that may decrease the interaction between preceding and following growth-layers and make a weak structural control, providing identical composition of growth layers in the case of the excess-Ca dolomite phase. As a result, layers with differing levels of excess Ca may occur, and interstratification of such layers form an irrational series of basal reflections. In particular, interstratification of layers of excess-Ca dolomite and of stoichiometric dolomite was determined, for example, in samples M236–034 (Table 8). It is possible that this two-component structural model significantly simplifies the actual more complex distribution of layers having different levels of excess Ca.

Searl (1994) and Jones *et al.* (2001) confined their study of compositional heterogeneity in dolomite to BSE analysis without a detailed XRD study of the coexisting phases. In the present work, application of both electron microprobe and XRD techniques provides a new level of information concerning the nature of heterogeneity in excess-Ca dolomite.

In fact, two levels of compositional heterogeneity are determined by these techniques. One of them is related to compositional zonation responsible for the existence of phases I and II that have significantly contrasting BSE intensity. A second, finer level of compositional heterogeneity exists within phases I and II. For example, the average contents of Ca in different zones of sample M236–116 are equal to 1.066, 1.092, 1.106, and 1.130. The differences between 1.066, 1.092, 1.106 and 1.130 exceed the experimental errors. At the same time, according to the XRD pattern, sample M236–116 consists of two phases, each of which is described by a periodic lattice. To account for this apparent contradiction between results obtained by the two techniques, two possibilities should be considered. The first applies where domains of different compositions coexist within the same zone and have coherent boundaries with the host structure, as was observed for the single crystals of sample M236–098. In this case, X-ray diffraction averages the cation composi-

tions of the different domains within the whole zone. The second case occurs where zones having different compositions scatter X-rays independently from each other. Thus, phases I and II of sample M236–116 in fact are physical mixtures of zones or domains where the amounts of Ca are equal to 1.066 *apfu* in phase I, and 1.092, 1.106, and 1.130 *apfu* in phase II. Assuming a linear relationship between the unit-cell parameters and the mole % CaCO₃ in excess-Ca dolomite, we expect unit-cell parameters for the pairs of domains forming phase I and II to be close to the following values: $a'_1 = 4.816$, $c'_1 = 16.063$ Å (phase I), and $a''_2 = 4.825$, $c''_2 = 16.124$, $a'''_2 = 4.827$, $c'''_2 = 16.147$ Å, and $a''''_2 = 4.834$, $c''''_2 = 16.185$ Å (phase II).

Assuming 40% of phase I and an equal probability of occurrence of the crystals or zones that differ slightly in the content of CaCO₃ for phase II, the statistically weighted parameters of the unit cells of phases I and II will be: $a_1 = 4.816$, $c_1 = 16.063$ Å and $a_2 = 4.829$, $c_2 = 16.152$ Å. These values almost coincide with the experimental ones (Table 3).

Figure 11 shows the XRD pattern calculated for the four structural models of excess-Ca dolomite having unit-cell parameters and concentrations given above. One can see that at the qualitative level, the calculated XRD pattern is similar to the experimental ones recorded for sample M236–116 because of the bimodal distribution of intensity in reflections having the same *hkl*.

Similarly, the compositional zones determined for sample M236–081 with mean Ca contents equal to 1.010, 1.046, 1.066, and 1.108 (Tables 9, 10) correspond to the three phases determined by XRD (Fig. 8a) because the XRD patterns from zones having 1.046 and 1.066 atoms of Ca overlap. Thus, because of the ability of X-ray diffraction to average structural parameters, each monophase identified by XRD corresponds to an assemblage of coherent scattering domains (CSDs) having close, but not identical levels of excess Ca. The variation in Ca uptake is accompanied by broadening of *hkl* reflections. However, the actual distribution of Ca in different zones or microcrystals cannot be determined because the broadening of *hkl* reflections depends also on the strain, size and distribution of CSDs. Therefore, Ca content determined by single-crystal refinements or the Rietveld technique is a statistically weighted content of Ca in different zones of single crystals or CSDs, which contribute to the formation of the XRD pattern.

A remarkable feature of the samples studied is that BSE-visible zones in coarse and fine crystals of the same sample have similar composition (Tables 9, 10). For example, for sample M236–116, Ca contents determined for the coarse crystals (1.068, 1.092 and 1.130 *apfu*) are exactly the same as those determined for the micritic portions of the sample (1.066, 1.092 and 1.130 *apfu*). This is a surprising result because the compositional zones and the crystals of different sizes, but having the same excess of Ca, had to have grown

in different conditions. Presumably, coarse crystals had more free space for their growth, whereas the fine crystals were formed in a local medium, possibly with lower permeability and, potentially, lower water:rock ratio. It is likely that coarse and fine crystals may have had different rates of growth.

However, the similarity of Ca-excess in crystals of both sizes indicates growth that is governed by the same or similar physical, chemical and crystal-chemical factors. Thus, there are two interrelated questions in the interpretation of the observed results: first, what factors are responsible for the compositional gap across domains in these crystals, and second, why do some domains of the large crystals and micritic material have the same or similar composition? We offer two possible answers to the first question. One is that growth of two different compositional zones in the large crystals and the micritic material took place in the presence of two different fluid phases.

Uniform stable isotopic composition of excess-Ca dolomite of different grain-size from the M236 core containing the monophase and two-phase samples studied suggests, however, that the polymodal dolomite composition is not likely related to contrasting composition of bulk fluid (Table 11). To explain the observed compositional gaps in the large and small crystals, considering the similar isotopic composition of the samples, it is reasonable to postulate that both types of crystals formed from the same fluid.

However, the fluid was locally heterogeneous with respect to the concentration of the “building material” (Ca, Mg, CO₃) in solution. Probably local fluctuations in concentration of the nutrients immediately around the growing crystals should be favorable for the formation of microcrystals with higher and lower excess Ca. One may assume that fluid forming the large and small crystals with a given excess in Ca was relatively uniform, and the size difference only relates to space available for growth. Perhaps the Ca content in the pore fluid fluctuated, and phase-I and phase-II dolomite grew at the same time into large and small crystals depending on the space available. In addition, formation of zones having different compositions may be controlled not only by local rhythmic changes in fluid composition around the surfaces of the growing crystals, but also by crystal-chemical constraints determining by formation the most stable arrangement of cations in the *B* layers.

Even with these two alternative assumptions, it is not clear what particular physical and chemical conditions induce the same discrete set of compositions of zones on both large crystals and micritic samples. Because of the large differences in burial history among the samples studied, it is unlikely that solution chemistry, degree of supersaturation, supply of nutrients, and other parameters controlling the crystal growth were the same near surfaces of both the finely dispersed and larger crystals during growth. It is thus probable that crystal-chemical constraints played a more significant role in formation

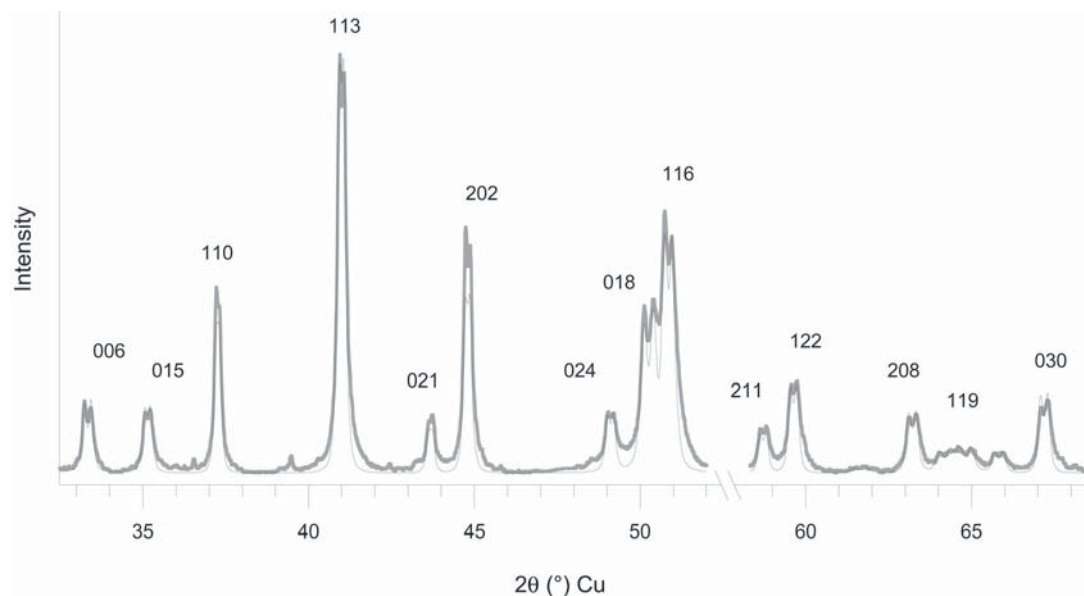


FIG. 11. Comparison of the experimental powder XRD pattern from sample M236-116 (shadow line) with that calculated for a mixture of four structural models for periodic excess-Ca dolomite, differing from each other by their unit-cell parameters (thin solid line) (for details, see the text).

TABLE 11. Sr, C, AND O ISOTOPE COMPOSITIONS FOR SAMPLES FROM THE DRINKARD FORMATION CORE, ALONG WITH OXIDE CONTENT FROM ICP ANALYSIS

Sample Analysis unit	⁸⁷ Sr/ ⁸⁶ Sr **	Na ₂ O %	MgO %	Al ₂ O ₃ %	SiO ₂ %	K ₂ O %	CaO %	TiO ₂ %	MnO %	Fe ₂ O ₃ %	Sr ppm	Ba ppm	Rb ppm	δ ¹³ C ‰ VPDB	δ ¹⁸ O
Detection limit		0.01	0.01	0.01	0.01	0.01	0.01	0.01	0.01	0.01	10	10	0.2		
M236-002	0.707505 ± 7	0.09	21.59	0.32	1.3	0.09	30.45	0.02	<0.01	0.17	53	18	2.9	4.34	-1.56
M236-081	0.707592 ± 7	0.12	18.78	0.66	0.9	0.08	32.84	0.01	0	0.15	181	33	0	5.07	-0.31
M236-098	0.707519 ± 7	0.04	19.37	0.46	0.7	0.06	32.32	0.01	0	0.12	98	26	0	4.55	-0.98
M236-118	0.707520 ± 8	0.08	18.55	0.28	1.48	0.08	33.55	0.02	<0.01	0.13	134	<10	3	4.49	-0.90
M236-122	0.707516 ± 8	0.10	18.87	0.21	1.49	0.06	34.60	0.01	<0.01	0.14	168	<10	1.9	4.83	-0.24
M236-124	0.707508 ± 7	0.18	18.30	0.72	2.61	0.16	32.00	0.02	0	0.19	203	22	0	5.16	0.76
M236-127	0.707484 ± 7	0.13	17.63	1.41	3.54	0.30	31.76	0.05	0	0.3	179	29	0	4.62	0.68

** reported uncertainties in measurement are 2 standard-error-of-the-mean values (*e.g.*, a reported uncertainty of ±7 is really ±0.000007). The two-sigma (95% confidence) reproducibility for the ⁸⁷Sr/⁸⁶Sr values is ±0.000016 (based on 41 analyses of the SRM 987 Sr standard within the past year, for which the mean value was 0.710266). Two-sigma reproducibility for the stable isotopic values for calcite are ±0.12 and ±0.18‰ for C and O, respectively (based on 49 analyses of an in-house marble standard). Dolomite samples probably have larger uncertainties. VPDB: Vienna PDB standard.

of the observed variations in extent of Ca-excess in both the large and small crystals.

POSSIBLE ORIGIN OF SPECIFIC DIFFRACTION- FEATURES, COMPOSITIONAL AND STRUCTURAL IMPERFECTIONS IN EXCESS-CA DOLOMITE

Reflection broadening and microstrain

An increase in the broadening of the *hkl* reflections with *l* for each given *hk*, as well as with (*h*² + *k*²) for each given *l*, is a characteristic feature of excess-Ca dolomite. Simulation of the experimental XRD patterns has shown that the broadening of reflections is associated with fluctuations in layer thickness and variations in the translations within the *ab* plane. Both these structural imperfections result from the local compositional heterogeneity of excess-Ca dolomite, leading to formation of microstrain. One of the main sources of microstrain in the structure of excess-Ca dolomite may be related to a tendency to mutual adjustment of the interstratified layers having different proportions of Ca in the *B* sites.

The presence of domains having δ, γ and ν structures and coherent boundaries with the host structure is another source of microstrain. The adjustment of the domains and host-matrix sizes should modify thickness of the layers in these structural fragments as well as provoke variations in the layer stacking within the *ab* plane. Finally, an overlap of closely located reflections having the same *hkl* and corresponding to microcrystals or some zones of the large crystals having slightly different levels of Ca-excess also results in broadening of the reflections, increasing with the diffusion vector

s ($s = 2\sin \theta/\lambda$). Formally, this effect mimics the broadening of reflections due to the fluctuations in layer thickness. The broadening of reflections observed in the experimental XRD patterns is successfully simulated using Δ*H* and Δ*t* values as variable parameters (Figs. 7, 8).

Calcite-like layers and their identification

One of the new diffraction features discovered in this study and characteristic of many samples of nonstoichiometric dolomite is that positions of the basal reflections deviate from those predicted by Bragg's law. The most plausible interpretation of this effect is that a few percent of 17.06 Å calcite-like layers are distributed among the host layers of the dolomite. The behavior of the basal reflections for such mixed-layer structures is in agreement with the rules of Méring (1949) and the experimental data.

According to these rules, basal reflections for a two-component structure are located between the 00*l* reflections of the nearest neighbor corresponding to periodic structures whose layers are interstratified. The width of the reflections increases with the distances between these neighboring 00*l* reflections, and their location depends on the proportion of the types of interstratified layers. Application of these rules to the mixed-layer excess-Ca dolomite – calcite shows that the nearest neighbor for the observed 006 reflection should be 006 reflection of excess-Ca dolomite with *d*(006) = 2.687 Å and calcite with *d*(006) = 2.843 Å. An increase of calcite layers should thus be accompanied by displacement of the 006 reflection of the mixed-layer phase toward low-2θ angles. In contrast, the observed 0012 reflection

of the mixed-layer phase has its nearest-neighbor 0012 peak of excess-Ca dolomite with $d(0012) = 1.3435 \text{ \AA}$ and 0013 maximum of calcite with $d(0013) = 1.3126 \text{ \AA}$. The calcite 0012 peak with $d = 1.4217 \text{ \AA}$ is located at a greater distance from the 0012 reflection of excess-Ca dolomite. As a result, the 0012 peak of the mixed-layer phase moves toward the high- 2θ angle with an increase in the proportion of calcite layers, as is observed in the calculated XRD patterns (Fig. 5a).

A small proportion of calcite-like layers in the host structure would be difficult to observe with HRTEM. However, even a small amount of calcite-like layers can significantly modify intensities, profiles and positions of the basal reflections. To illustrate, we compare in Figures 7b and 12 the experimental XRD pattern of sample M236-034 with those calculated using two different models. One of them consists of layers of interstratified excess-Ca dolomite, stoichiometric dolomite, and calcite, the structural parameters providing a satisfactory agreement with the experimental pattern (Fig. 7b, Table 8). The other one also consists of layers of Ca-rich and stoichiometric dolomite having the same structural and probability parameters as those in the previous model, but the absence of calcite-like layers

dramatically modifies the calculated XRD pattern in comparison with the experimental one.

One of the interesting questions related to the presence of calcite-like layers is whether these layers are commensurate or incommensurate in the ab plane with the layers of the host structure. Simulation of the experimental XRD patterns (Figs. 7, 8) was carried out assuming that both types of layers are commensurate. Two reasons justify this approach. First, the 17.06 \AA layers may have a cation proportion that differs from that of pure calcite. For example, these layers may contain in the B sites equal amounts of Ca and Mg. Second, a small amount of such layers should be separated from each other by a relatively thick stack of excess-Ca dolomite layers, having smaller a and c parameters. Therefore, to adjust their two-dimensional size to the host layers, the calcite-like layers of a $\text{Ca}_{1.5}\text{Mg}_{0.5}(\text{CO}_3)_2$ composition may decrease their two-dimensional size and increase the thickness up to 17 \AA .

However, even if the actual mixed-layer structures consist of incommensurate excess-Ca dolomite and calcite-like layers in the ab plane, the diffraction effects from these structures would be almost identical to those from the mixed-layer structure with the commensu-

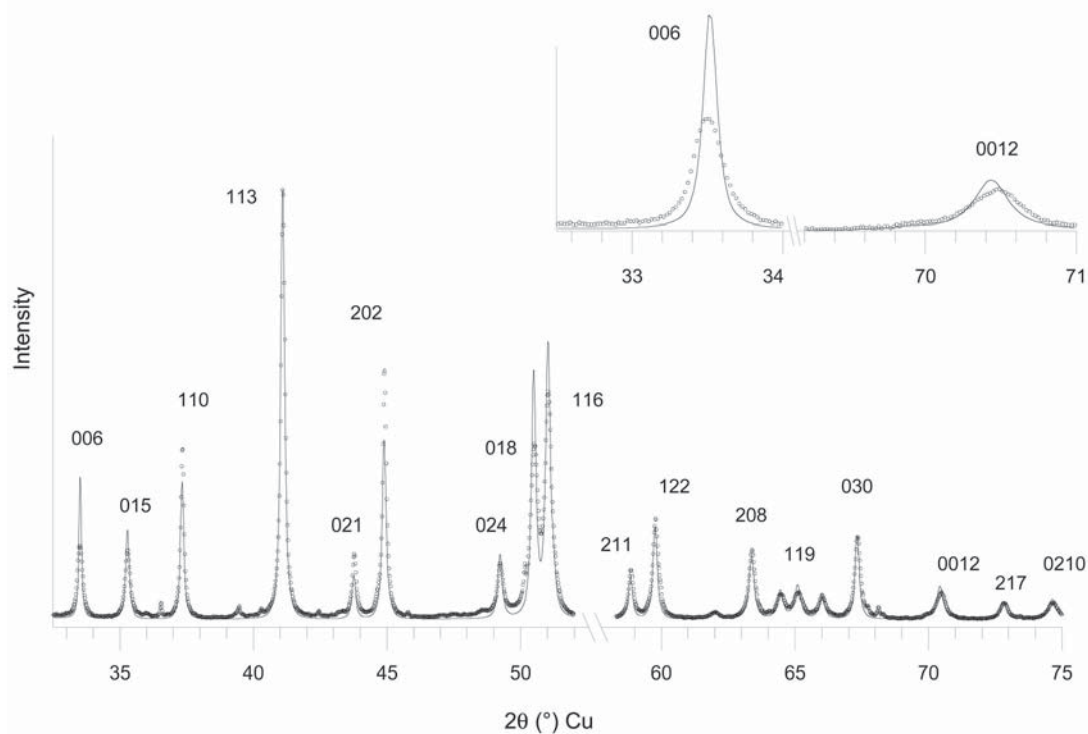


FIG. 12. Comparison of the experimental powder XRD patterns from sample M214-034 (dotted line) with that calculated for a calcite-free mixed-layer structure containing 89.6% of 16.034 \AA nonstoichiometric and 10.4% of stoichiometric dolomite layers (solid line) (see also Fig. 7b and Table 8).

rate layers containing a low amount of calcite-like layers. Indeed, a mixed-layer structure consisting of incommensurate excess-Ca dolomite and calcite-like layers can be considered as two substructures, each of which has its own two-dimensional periodicity. One of these substructures can be considered as a set of thin substacks consisting of identical excess-Ca dolomite layers that are separated from each other by 17.06 Å along the *c* axis.

The particular feature of this substructure is that the 17.06 Å interlayer spacings do not contain scattering matter. As in the case of non-rational basal reflections, an irregular distribution of the 17.06 Å interlayers within CSDs of the mixed-layer structure should modify three-dimensional coherent scattering of X-rays from adjacent substacks and change the positions, shapes and intensities of *hkl* reflections. The second substructure should consist of a few isolated calcite-like layers separated from each other by distances equal to the thickness of the individual layer substacks. A small amount of calcite layers in the mixed-layer phases studied, their irregular distribution, and their separation at large distances should provide a very small or even negligible contribution to the total diffraction effect from the structure.

The main difference between the model described and the model used in our calculations is that the empty 17.06 Å interlayers were replaced by actual layers of calcite. However, because of a very low content of calcite-like layers and their random distribution in the mixed-layer phases studied (2–4%), the XRD patterns from a mixed-layer excess-Ca dolomite – calcite with and without scattering matter in the 17.06 Å layers would be almost identical. This conclusion is confirmed by calculations of XRD patterns from such mixed-layer structural models differing from each other by the scattering powers of the 17.06 Å layers. XRD patterns from both models are indistinguishable.

The actual origin of single 17 Å calcite-like layers within excess-Ca dolomite is not clear. One may assume, however, that excess-Ca dolomite varieties were formed by pseudomorphic replacement of the calcite structure. To preserve the calcite matrix, Mg should replace Ca only in the *B* layer, with no replacement in the *A* sites, or in the *A* site with no replacement in the *B* site. Such a reaction should start from different parts of the calcite crystal, and even under strict structural control, a high probability should exist for compositional stacking faults providing an opportunity for single layers of calcite to survive in the newly formed excess-Ca dolomite structure.

Interstratification of layers of nonstoichiometric and stoichiometric dolomite

For some samples of monophase and two-phase excess-Ca dolomite, comparison of the experimental $d(hkl)$ with those calculated from the refined unit-cell

parameters shows that agreement between $d_{\text{exp}}(hkl)$ and $d_{\text{calc}}(hkl)$ depends on *l*. For small *l*, within experimental errors, there is agreement between the compared values. However, a significant disagreement between the compared values is observed for high values of *l*. Calculations of XRD patterns from different models show that this effect is characteristic of mixed-layer structures in which layers of nonstoichiometric and stoichiometric dolomite are interstratified.

To account for the different susceptibility of *hkl* reflections to 2θ migration, one has to consider that in the case of mixed-layer structures, the nature of diffraction effects for basal and non-basal reflections should be the same (Drits & McCarty 1996). Therefore, for each given *hk* rod in reciprocal space, *hkl* nodes from a two-component mixed-layer structure must be situated along this rod and between the most closely spaced *hkl* nodes corresponding to periodic structures that make up the interstratified layers. Let us assume a mixed-layer structure consisting of *m* and *n* interstratified layers. Where the content of the layers of one type (*e.g.*, *n* type) increases, each *hkl* node corresponding to the mixed-layer structure migrates from the *hkl* node of the periodic structure consisting of *m* layers toward the nearest *hkl* node of the periodic structure consisting of the *n* layers. The value of the shift depends on the content of the *n* layers and distances between the nearest *hkl* nodes corresponding to the two periodic structures. This dependence can be expressed by a simple relationship, $y = W_n Z$, in which *y* is the distance in reciprocal space between a node corresponding to the mixed-layer structure and the nearest $(hkl)_m$ node corresponding to the periodic structure consisting of the *m* layers; W_n is the proportion of *n* layers, and *Z* is the distance in reciprocal space between the nearest *hkl* nodes corresponding to the two periodic structures between which the node corresponding to the mixed-layer structure is located. Thus, at each given W_n , the higher *l* for the nearest *hkl* nodes corresponding to the periodic structures, the longer the distances between them, *i.e.*, *Z* values, and therefore the greater the shift of the nodes corresponding to the mixed-layer structures. Simulation of the experimental XRD patterns from excess-Ca dolomite confirms the occurrence of the mixed-layer structures, at least in some of the samples studied.

CONCLUSIONS

Crystal structures of excess-Ca dolomite refined by the single-crystal diffraction method (Reeder 2000) and by the Rietveld technique show that there are two distinct varieties, each of which is characterized by a 3D periodic lattice. In one of them, both the *A* and *B* sites of the average unit-cell have a mixed proportion of Ca and Mg cations. In the other one, the excess Ca is located in the *B* layers, whereas the *A* sites are occupied only by Ca. The Ca-excess only in the *B* layers is consistent with the domain model of excess-Ca dolomite based on

the SAED and TEM observations. A mixed proportion of cations in both the *A* and *B* sites in the average unit-cell requires either a mixed-cation occupancy of both these sites in the host structure or the existence of some new domains with the new distribution of Ca and Mg in the *A* and *B* sites.

We found that the different occupancy of cations in the *A* and *B* sites in the average unit-cells of excess-Ca dolomite results in different relationships between their unit-cell parameters. Diffraction criteria for identification of excess-Ca dolomite having a mixed Ca,Mg occupancy only in the *B* or in both *A* and *B* sites are provided.

It is likely that the phase composition of excess-Ca dolomite depends on the total amount of Ca-uptake in the structure. From the XRD point of view, excess-Ca dolomite in which Ca does not exceed 1.05 *apfu* usually forms a single phase. In contrast, excess-Ca dolomite containing higher total content of Ca ($n_{Ca} > 1.05$ *apfu*) typically consists of at least two dolomite phases differing from each other in the extent of excess Ca uptake.

There are different levels of compositional heterogeneity of such two-phase excess-Ca dolomite. One of them is related to the significantly different extent of excess Ca in the coexisting phases, so that the XRD patterns of such samples consist of visually resolved reflections having the same *hkl*. A finer level of compositional heterogeneity includes a set of microcrystals, or zones within coarse crystals of dolomite, in which the difference in excess Ca is so small that the reflections from these microcrystals and zones having the same *hkl* overlap, forming single diffraction-maxima. This effect imitates reflection broadening due to fluctuations in layer thickness. Both levels of compositional heterogeneity are observed for coarse crystals of excess-Ca dolomite. To account for the compositional gap across zones in the excess-Ca dolomite crystals, as well as the same or similar cation proportions in micritic domains and some zones of the large crystals, we propose a model for formation of excess-Ca dolomite. We assume that bulk fluid composition was the same, but Ca:Mg ratio fluctuated locally, and phase-I and phase-II excess-Ca dolomite grew at the same time in large and small crystals depending on the space available for growth.

In agreement with Searl (1994), we assume that the growth of crystals of excess-Ca dolomite is restricted to certain cation proportions in which the tendency to an ordered distribution of Ca and Mg in the *B* layers is possible. It is likely that this cation order is one of the essential factors responsible for persistence or relative stability of Ca-rich dolomite through various diagenetic conditions.

Along with domains having δ , ν , and γ structures, additional sources may be responsible for the uptake of excess Ca into excess-Ca dolomite. One of them is related to the presence of calcite-like layers. Even a few percent of these layers provides a significant contribu-

tion to the total amount of Ca. Another source of excess Ca may be layers of nonstoichiometric dolomite, which can form individual homogeneous microcrystals, or zones in coarse single crystals, or interstratify with layers of stoichiometric dolomite. The presence of calcite-like layers in excess-Ca dolomite, as well as interstratification of layers of nonstoichiometric and stoichiometric dolomite, can be easily identified by the diffraction criteria described above.

Simulation of the experimental XRD patterns carried out for the first time for excess-Ca dolomite shows that their defective structures can be described in terms of a mixed-layer model in which calcite-like layers, layers of nonstoichiometric dolomite, and layers of stoichiometric dolomite are randomly interstratified.

ACKNOWLEDGEMENTS

The authors extend special thanks to Drs. J. Bergman and R. Kleeberg for their generous help and advice with Rietveld analysis. Financial support was provided by ChevronTexaco and sample preparation by Russell Anderson, who deserves thanks. VAD and BAS thank the Russian Fund of Fundamental Research. We are grateful to the reviewers, Holger Lindgren and Duncan Sibley, for their helpful comments, and especially to the Editor, Robert F. Martin, who helped significantly to improve the manuscript.

REFERENCES

- ANTAO, S.M., MULDER, W.H., HASSAN, I., CRICHTON, W.A. & PARISE, J.B. (2004): Cation disorder in dolomite, $\text{CaMg}(\text{CO}_3)_2$, and its influence on the aragonite + magnesite \leftrightarrow dolomite reaction boundary. *Am. Mineral.* **89**, 1142-1147.
- BARBER, D.J., REEDER, R.J. & SMITH, D.J. (1985): A TEM microstructural study of dolomite with curved faces (saddle dolomite). *Contrib. Mineral. Petrol.* **91**, 82-92.
- BERGMAN, J. & KLEEBERG, R. (1998): Rietveld analysis of disordered layer silicates. *Materials Science Forum* **278-281**(1), 300-305.
- _____, _____, HAASE A. & BREIDENSTEIN, B. (2000): Advanced fundamental parameter model for improved profile analysis. *Materials Science Forum* **347-349**(2), 303-308.
- BLAKE, D.F., PEACOR, D.R. & WILKINSON, B.H. (1982): The sequence and mechanism of low-temperature dolomite formation: calcian dolomite in a Pennsylvanian echinoderm. *J. Sed. Petrol.* **52**, 59-70.
- BRADLEY, W.F., BURST, J.F. & GRAF, D.L. (1953): Crystal chemistry and differential thermal effects of dolomite. *Am. Mineral.* **38**, 207-217.
- BRAUNBARTH, C., HILLHOUSE, H.W., NAIR, S., TSAPATIS, M., BURTON, A., LOBO, R.F., JACUBINAS, R.M. & KUZNICKI,

- S.M. (2000): Structure of strontium-ion-exchanged ETS-4 microporous molecular sieves. *Chem. Materials* **12**, 1857-1865.
- BUDD, D.A. (1997): Cenozoic dolomites of carbonate islands: their attributes and origin. *Earth-Sci. Rev.* **42**, 1-47.
- CHAI, L., NAVROTSKY, A. & REEDER, R.J. (1995): Energetics of calcium-rich dolomite. *Geochim. Cosmochim. Acta* **59**, 939-944.
- CUADROS, J. & ALTANER, S.P. (1998): Compositional and structural features of the octahedral sheet in mixed-layer illite smectite from bentonites. *Eur. J. Mineral.* **10**, 111-124.
- DRITS, V.A., LANSON, B., GORSHKOV, A.I. & MANCEAU, A. (1998): Substructure and superstructure of four-layer Ca-exchanged birnessite. *Am. Mineral.* **83**, 97-118.
- _____ & MCCARTY, D.K. (1996): The nature of diffraction from illite and illite-smectite consisting of interstratified trans-vacant and cisvacant 2:1 layers: a semiquantitative technique determination of layer-type content. *Am. Mineral.* **81**, 852-863.
- _____ & SAKHAROV, B.A. (1976): *X-ray Structural Analysis of Mixed-Layer Minerals*. Nauka, Moscow, Russia (in Russ.).
- _____, ŚRODOŃ, J. & EBERL, D.D. (1997): XRD measurement of mean crystallite thickness of illite and illite/smectite: reappraisal of the Kubler index and the Scherrer equation. *Clays Clay Minerals* **45**, 461-473.
- _____ & TCHOUBAR, C. (1990): *X-ray Diffraction of Disordered Lamellar Structures. Theory and Application to Microdivided Silicates and Carbons*. Springer Verlag, New York, N.Y.
- _____, WEBER, F., SALYN, A.L. & TSIPURSKY, S.I. (1993): X-ray identification of 1M illite varieties. *Clays Clay Minerals* **41**, 389-398.
- EFFENBERGER, H., MEREITER, K. & ZEMANN, J. (1981): Crystal structure refinements of magnesite, calcite, rhodochrosite, siderite, smithsonite, and dolomite, with discussion of some aspects of the stereochemistry of calcite-type carbonates. *Z. Kristallogr.* **156**, 233-243.
- FOUKE, B.W. & REEDER, R.J. (1992): Surface structural controls on dolomite composition: evidence from sectoral zoning. *Geochim. Cosmochim. Acta* **56**, 4015-4024.
- FÜCHTBAUER, H. & GOLDSMITH, J.R. (1965): Beziehungen zwischen Calciumgehalt und Bildungsbedingungen der Dolomite. *Geol. Rundschau* **55**, 29-40.
- GAILLOT, A.C., DRITS, V.A., PLANÇON, A. & LANSON, B. (2004): Structure of synthetic K-rich birnessites obtained by high-temperature decomposition of KMnO_4 . 2. Phase and structural heterogeneities. *Chem. Materials* **16**, 1890-1905.
- GOLDSMITH, J.R. & GRAF, D.L. (1958): Structural and compositional variations in some natural dolomites. *J. Geol.* **66**, 678-693.
- GRAF, D.L. (1961): Crystallographic tables for the rhombohedral carbonates. *Am. Mineral.* **46**, 1283-1316.
- _____ (1969): Crystallographic tables for the rhombohedral carbonates: a correction. *Am. Mineral.* **54**, 325.
- _____, BLYTH, C.R. & STEMMLER, R.S. (1967): One-dimensional disorder in carbonates. *Illinois State Geol. Surv., Circ.* **408**, 1-60.
- GREGG, J.M., HOWARD, S.A. & MAZZULLO, S.J. (1992): Early diagenetic recrystallization of Holocene (<3000 years old) peritidal dolomites, Ambergris Cay, Belize. *Sedimentology* **39**, 143-160.
- GUALTIERI, A.F. (1999): Modeling the nature of disorder in talc by simulation by X-ray powder diffraction. *Eur. J. Mineral.* **11**, 521-532.
- GUINIER, A. (1964): *Theorie et technique de la radiocristallographie. Chap 13: Diffraction par les réseaux cristallins imparfaits*. Dunod, Paris, France (490-636).
- HOWIE, R.A. & BROADHURST, F.M. (1958): X-ray data for dolomite and ankerite. *Am. Mineral.* **43**, 1210-1214.
- JONES, B., LUTH, R.W. & MACNEIL, A.J. (2001): Powder X-ray diffraction analysis of homogeneous and heterogeneous sedimentary dolostones. *J. Sedimen. Res.* **71**, 790-799.
- LAND, L.S. (1980): The isotopic and trace element geochemistry of dolomite: the state of the art. In *Concepts and Model of Dolomitization* (D.H. Zenger, J.B. Dunham & R.L. Ethington, eds.). *Soc. Econ. Geol., Paleontol., Mineral., Spec. Publ.* **28**, 87-110.
- LANSON, B., DRITS, V.A., GAILLOT, A.-C., SILVESTER, E., PLANÇON, A. & MANCEAU, A. (2002): Structure of heavy metal sorbed birnessite. I. Results from X-ray diffraction. *Am. Mineral.* **87**, 1631-1645.
- _____, _____, SILVESTER, E. & MANCEAU, A. (2000): Structure of H-exchanged hexagonal birnessite and its mechanism of formation from Na-rich monoclinic busserite at low pH. *Am. Mineral.* **85**, 826-838.
- LEONI, M., GUALTIERI, A.F. & ROVERI, N. (2004): Simultaneous refinement of structure and microstructure of layered materials. *J. Appl. Crystallogr.* **37**, 166-173.
- LIPPMANN, F. (1973): *Sedimentary Carbonate Minerals*. Springer-Verlag, Berlin, Germany.
- LUMSDEN, D.N. (1979): Discrepancy between thin-section and X-ray estimates of dolomite in limestones. *J. Sed. Petrol.* **49**, 429-436.
- MANCEAU, A., DRITS, V.A., SILVESTER, E., BARTOLI, C. & LANSON, B. (1997): Structural mechanism of Co^{2+} oxida-

- tion by the phyllosilicate busierite. *Am. Mineral.* **82**, 1150-1175.
- _____, LANSON, B., DRITS, V.A., CHATEIGNER, D., GATES, W.P., WU, J., HUO, D. & STUCKI, J.W. (2000): Oxidation-reduction mechanism of iron in dioctahedral smectites. I. Crystal chemistry of oxidized reference nontronites. *Am. Mineral.* **85**, 133-152.
- MAZZULLO, S.J. (1992): Geochemical and neomorphic alteration of dolomite: a review. *Carbonates and Evaporites* **7**, 21-37.
- MCCARTY, D.K. & REYNOLDS, R.C., JR. (1995): Rotationally disordered illite smectite in Paleozoic K-bentonites. *Clays Clay Minerals* **43**, 271-284.
- _____, & _____ (2001): Three-dimensional crystal structures of illite-smectite minerals in Paleozoic K-bentonites from the Appalachian basin. *Clays Clay Minerals* **49**, 24-35.
- MÉRING, J. (1949): L'interférence des rayons X dans les systèmes à stratification désordonnée. *Acta Crystallogr.* **2**, 371-377.
- MISER, D.E., SWINNEA, J.S. & STEINFINK, H. (1987): TEM observations and X-ray crystal-structure refinement of a twinned dolomite with a modulated structure. *Am. Mineral.* **72**, 188-193.
- NAVROTSKY, A. & CAPOBIANCO, C. (1987): Enthalpies of formation of dolomite and of magnesian calcite. *Am. Mineral.* **72**, 782-787.
- NEWSAM, J.M. & TREACY, M.M.J. (1993): ZeoFile: a stack of zeolite structure types. *Zeolites* **13**, 183-186.
- PLANÇON, A. (1981): Diffraction by layer structures containing different kinds of layers and stacking faults. *J. Appl. Crystallogr.* **14**, 300-304.
- _____, (2002): New modeling of X-ray diffraction by disordered lamellar structures, such as phyllosilicates. *Am. Mineral.* **87**, 1672-1677.
- _____, GIESE, R.F., SNYDER, R., DRITS, V.A. & BOOKIN, A.S. (1989): Stacking faults in the kaolin-group minerals: defect structures of kaolinite. *Clays Clay Minerals* **37**, 203-210.
- _____, & TCHOUBAR, C. (1977): Determination of structural defects in phyllosilicates by X-ray powder diffraction. I. Principle of calculation of the diffraction phenomenon. *Clays Clay Minerals* **25**, 430-435.
- REEDER, R.J. (1981): Electron optical investigation of sedimentary dolomites. *Contrib. Mineral. Petrol.* **76**, 148-157.
- _____, (1983): Crystal chemistry of the rhombohedral carbonates. In *Carbonates; Mineralogy and Chemistry* (R.J. Reeder, ed.). *Rev. Mineral.* **11**, 1-47.
- _____, (1992): Carbonates; growth and alteration microstructures. In *Minerals and Reactions at the Atomic Scale; High Resolution Transmission Electron Microscopy* (P.R. Buseck, ed.). *Rev. Mineral.* **27**, 380-424.
- _____, (2000): Constraints on cation order in calcium-rich sedimentary dolomite. *Aquatic Geochem.* **6**, 213-226.
- _____, & DOLLASE, W.A. (1989) Structural variation in the dolomite-ankerite solid-solution series: an X-ray, Mössbauer, and TEM study. *Am. Mineral.* **74**, 1159-1167.
- _____, & WENK, H.-R. (1979): Microstructures in low temperature dolomites. *Geophys. Res. Lett.* **6**, 77-80.
- _____, & _____ (1983): Structure refinements of some thermally disordered dolomites. *Am. Mineral.* **68**, 769-776.
- REKSTEN, K. (1990): Superstructures in calcian ankerite. *Phys. Chem. Minerals* **17**, 266-270.
- REYNOLDS, R.C., JR. (1993): Three-dimensional X-ray powder diffraction from disordered illite: simulation and interpretation of the diffraction patterns. In *Computer Applications to X-Ray Diffraction Analysis of Clay Minerals* (R.C. Reynolds Jr. & J.R. Walker, eds.). *Clay Minerals Soc., Workshop Lectures* **5**, 43-78.
- RIETVELD, H. (1969): A profile refinement method for nuclear and magnetic structures. *J. Appl. Crystallogr.* **2**, 65-71.
- SAKHAROV, B.A., BESSON, G., DRITS, V.A., KAMENEVA, M.Y., SALYN, A.L. & SMOLIAR, B.B. (1990): X-ray study of the nature of stacking faults in the structure of glauconites. *Clay Minerals* **25**, 419-435.
- _____, NAUMOV, A.S. & DRITS, V.A. (1982): X-ray diffraction by mixed-layer structures with random distribution of stacking faults. *Dokl. Akad. Nauk SSSR* **265**, 339-343 (in Russ.).
- SEARL, A. (1994): Discontinuous solid solution in Ca-rich dolomites: the evidence and implications for the interpretation of dolomite petrographic and geochemical data. In *Dolomites: a Volume in Honour of Dolomieu* (B. Purser, ed.). *Int. Assoc. Sedimentol., Spec. Publ.* **21**, 361-376.
- _____, & FALLICK, A.E. (1990): Dinantian dolomites from East Fife: hydrothermal overprinting of early mixing zone stable isotopic and Fe/Mn compositions. *J. Geol. Soc. London* **147**, 623-638.
- SPERBER, C.M., WILKINSON, B.H. & PEACOR, D.R. (1984): Rock composition, dolomite stoichiometry and rock/water reactions in dolomitic carbonate rocks. *J. Geol.* **92**, 609-622.
- STEINFINK, H. & SANS, F.J. (1959): Refinement of the crystal structure of dolomite. *Am. Mineral.* **44**, 679-682.
- VAN TENDELOO, G., WENK, H.-R. & GRONSKY, R. (1985): Modulated structures in calcian dolomite: a study by electron microscopy. *Phys. Chem. Minerals* **12**, 333-341.

- WENK, H.-R., BARBER, D.J. & REEDER, R.J. (1983): Microstructures in carbonates. *In* Carbonates: Mineralogy and Chemistry (R.J. Reeder, ed.). *Rev. Mineral.* **11**, 301-367.
- _____, HU, MEISHENG, LINDSEY, T. & MORRIS, H.W., JR. (1991): Superstructures in ankerite and calcite. *Phys. Chem. Minerals* **17**, 527-539.
- _____ & ZHANG, F. (1985): Coherent transformations in calcian dolomites. *Geology* **13**, 457-460.
- YLAGAN, R.F., ALTANER, S.P. & POZZUOLI, A. (2000): Reaction mechanisms of smectite illitization associated with hydrothermal alteration from Ponza Island, Italy. *Clays Clay Minerals* **48**, 610-631.

Received December 7, 2004, revised manuscript accepted June 25, 2005.